Z. Angew. Math. Phys. (2022) 73:78

0044-2275/22/020001-26
published online March 28, 2022
https://doi.org/10.1007/s00033-022-01715-x

Zeitschrift für angewandte Mathematik und Physik ZAMP

A new deformation measure for the nonlinear micropolar continuum

Gabriele La Valle

Abstract. The possibility to introduce a new relative rotation tensor in the field of nonlinear micropolar continua is discussed in the present paper. The proposed deformation tensor is able to uncouple the classic energetic contribution, related to the material particles translation, and the non-classic ones due to the material particles microrotation. The two main used tool are the least action principle and Levi–Civita absolute tensor calculus which allow to derive the new Euler–Lagrange equations. Some numerical applications are made to investigate the mathematical and mechanical implications of the proposed theoretical model. Axial, bending and torsion numerical tests are performed on structural elements typical of a pantographic structure. Interesting behaviours have been obtained which cannot be forecasted by classical elasticity. In addition of predicting new phenomena, it follows that the new relative rotation tensor could help in the description of granular materials and in the design of novel metamaterials that could be macroscopically described by means of the proposed tensor itself.

Mathematics Subject Classification. 74B20.

1. Introduction

Micropolar elasticity differs from classical elasticity in that in the first one each material particle cannot only translate, but also independently rotate. The first ideas about the micropolar continuum were summarized by the Cosserat brothers [1], and later results in the field of nonlinear micropolar continua were obtained by Eremeyev et al. [2], Altenbach et al. [3,4], Forest [5], dell'Isola and Eremeyev [6], Eremeyev and Pietraszkiewicz [7]. Micropolar theories are strictly related to the second gradient ones in which the specific deformation energy is expressed as a function of the second displacement gradient; although a complete work on this relationship has not yet been published, Bersani et al. [8] have drawn the path to follow to link them with each other by means of the Lagrange multiplier theorem: a review on the Lagrange multiplier theorem can be found in dell'Isola and Di Cosmo [9]. Historically, a precursor of higher-order theories can be considered Gabrio Piola whose work has been translated in two volumes by dell'Isola et al. [10,11], in a paper by dell'Isola et al. [12] and an analysis of its legacy can be found in [13,14]; on the other hand, some recent theoretical and numerical studies on the topic have been made by Auffray et al. [15], dell'Isola and Seppecher [16,17], Seppecher [18] and Andreaus et al. [19].

A careful review of the reference literature shows the presence of two distinct groups of scientists belonging to two different schools of thought: continuum thermodynamics and analytical continuum mechanics. They are the result of two different postulation schemes to develop models: the first starts from the balance of forces and equilibrium equations; the second focuses on the least action principle or, more generally, on the principle of virtual work. It is precisely the difficulty encountered in overcoming classical elasticity that led to reflect on the fundamental aspects of mechanics. We can refer to the works by Eugster and dell'Isola [20–22] in which an exegesis of significant historical articles can be found; to the treatments by Germain [23], Barchiesi et al. [24], dell'Isola and Placidi [25] about the method of virtual work in the mechanics of continuous and its potential to create new theories.

The development of new models and theories is not only theoretical speculation, but it can practically impact in two main fields: the description of the ever-increasing number of new materials; the creation of new metamaterials that follow a fixed new theoretical model. In this regard, a paradigmatic case is offered by pantographic structures [26–29]. Pantographic structures consist of a planar grid obtained by superposition of two families of bars that are connected by small cylinders usually called pivots. Their history is closely linked to two main aspects: the development of second gradient continua and the development of the 3D printing technology (see Gołaszwski et al. [30]); both led to deep and serious scientific remarks. A review on metamaterials can be found in Barchiesi et al. [31,32] and a review of some relevant approaches for designing bio-metamaterials can be found in Giorgio et al. [33]; instead, among all the numerous works about pantographic structures, we need to mention those by Alibert et al. [34], dell'Isola et al. [35,36] and Eremeyev et al. [37]. Recently, Ciallella et al. [38] analytically and experimentally investigate the cyclic behaviour and dissipative properties of pantographic fabrics; Giorgio [39] generalizes the idea of a pantographic sheet to obtain a more general elastic model for nets made up of two families of curved Kirchhoff rods. In this context, we need to mention the work by Greco [40] where an iso-parametric conforming finite element formulation is presented for the analysis of Kirchhoff rods in the planar 2D case.

Pantographic structures have been studied from different points of view and different kind of modelling: in addition to a meso-model in which they are considered as an assembly of Euler–Bernoulli beams characterized by axial, bending, and torsional stiffness constitutive parameters [41], there exists the Piola–Hencky-type Lagrangian model in which the mechanical behaviour of the microstructure is synthetically described as a set of extensional springs interconnected by two other families of rotational springs for involving bending and shear effects [42–45]; both microscopic discrete models tend to 2D continuum models depending on the second in-plane displacement gradient [46,47].

Besides the potential to create new kinds of metamaterials, continuum and discrete micropolar models have already been applied for the analysis of granular materials by Misra et al. [48–50], Giorgio et al. [51,52], Turco et al. [53] and for the mechanical description of fibre reinforced solids by Steigmann [54], Shirani and Steigmann [55]. Some stochastic considerations have been taken into account by Trovalusci et al. [56]; others should be added involving simplified Monte Carlo simulations for finite element discretized structures [57–59], random matrices [60], the probability transformation method [61–64] and mixed probabilistic approaches [65–67].

In this paper, a new deformation measure related to the difference between micro- and macrorotation is introduced. A complete list of the independent deformation measures used in the literature in the field of nonlinear micropolar continua can be found in Pietraszkiewicz and Eremeyev [68,69]: relative stretch and wryness tensors are considered. The stretch tensor is frequently supposed to be dependent on the product between the transposed of the microrotation tensor and the gradient of the placement function; therefore, it is commonly assumed to be a function of the macrorotation tensor and of the square root of the Cauchy-Green tensor. The deformation energy density derived from the aforementioned tensors makes it difficult to distinguish classic and non-classic energetic contributions and/or effects under the hypothesis of large displacements. The previous consideration led the author to introduce a new relative rotation tensor, which, together with the Green–Saint–Venant tensor and the usual wryness tensor, allows to highlight three different kind of strain.

Some numerical applications are performed to analyse the main features of the proposed model. Rectangular and cylindrical beams typical of a pantographic sheet are studied by means of a deformation energy density derived under the hypotheses of large displacements and isotropic materials. Since only two of the three considered deformation tensors are independent, the chosen energy can be seen as a particular form of constitutive equations of a classic micropolar model where only two independent deformation measures appear. The relationship between the introduced constitutive parameters and the classic micropolar ones is shown. Some peculiar effects are obtained. As the constitutive parameter linked to the skewsymmetric part of the new relative rotation tensor increases, we can underline a significant reduction in the portion of the beams characterized by transversal displacements different from zero if an axial displacement is imposed; an inversion of compressed and stretched fibres after a bending caused by

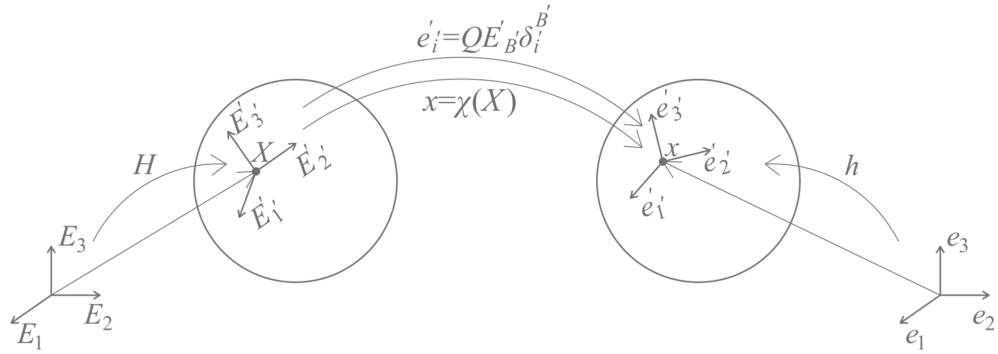

FIG. 1. Physical significance of χ, H, h and Q

transversal displacements; a reduction in the area of the sample affected by transversal displacements if torsional displacements are imposed. We can conclude that the deformation measure introduced in this work could help with modelling of complex materials.

2. Kinematics of the micropolar continuum

Let $\mathcal{V}$ and $\mathcal{V}^*$ be two vector spaces. Hereafter, the symbol $Lin\,(\mathcal{V},\mathcal{V}^*)$ represents the set of linear applications which arrange an element of $\mathcal{V}$ to an element of $\mathcal{V}^*$; the symbols $Ort\,(\mathcal{V},\mathcal{V}^*)$ and $Sym\,(\mathcal{V},\mathcal{V}^*)$ stand for the sets of linear orthogonal and symmetric applications from $\mathcal{V}$ to $\mathcal{V}^*$, respectively. The Levi–Civita absolute tensor calculus have been used; upper case letters to indicate components in the Lagrangian space and lower case letters to indicate components in the Eulerian space have been chosen. The determinant of a linear application has been denoted $det\,[\cdot]$; finally, the symbol δ denotes the Kronecker delta: δ_N^M, δ_{MN} and δ_N^M are equal to 1 if $M = N$; equal to zero, otherwise.

Let $\mathcal{L}$ be the initial (or Lagrangian) configuration and let $\mathcal{E}$ be the current (or Eulerian) configuration. According to Cosserat and Cosserat [1], each material particle is characterized by six degrees of freedom. Then, in the reference placement, the state of each particle is described by a position vector $X \in \mathcal{L}$ and by a local reference system defined by three vectors

$$E'_{A'}\,(X) = H\,(X)\,E_A \tag{1}$$

where $E_A \in \mathcal{L}$ are orthonormal base vectors of $\mathcal{L}$ and the application $H \in Ort\,(\mathcal{L},\mathcal{L})$ is such that

$$H^{-1} = H^T;\ det[H] = 1 \tag{2}$$

In the current configuration, each particle is identified by means of:

- the field $\chi : \mathcal{L} \to \mathcal{E}, x = \chi(X,t)$ which denotes the placement field between $\mathcal{L}$ and $\mathcal{E}$;
- the application $Q \in Ort\,(\mathcal{L},\mathcal{E})$ which describes the difference between the initial and the current orientation of the local reference system able to fix the orientation of each particle:

$$e'_{i'}(X,t) = Q(X,t)E'_{B'}(X)\delta_{i'}^{B'} \tag{3}$$

  where $e'_{i'}\,(X) = h\,(X)\,e_i$; e_i are orthonormal base vectors of $\mathcal{E}$; $h \in Ort\,(\mathcal{E},\mathcal{E})$ and $det[h] = 1$; the application Q is assumed to have the properties

$$Q^{-1} = Q^T;\ det[Q] = 1 \tag{4}$$

The field χ and the tensor Q are supposed to be independents. In Fig. 1, the physical significance of χ, H, h, and Q has been clarified.

2.1. Deformation measures

In this section, the Green–Saint–Venant tensor and the common wryness tensor are briefly recalled; moreover, a new deformation measure is introduced which is able to discouple classic and non-classic mechanical effects. All the deformation measures have to be the same in two configurations that differ only for a rigid act of motion. In other words, they need to be objective in a sense that is shown in Sect. 2.2.

2.1.1. Green–Saint–Venant tensor. Let be $F = \nabla_X \chi$ the placement gradient which belongs to $Lin(\mathcal{L}, \mathcal{E})$. The polar decomposition theorem ensures the existence of only one couple of linear applications $(R, U) \in Ort(\mathcal{L}, \mathcal{E}) \times Sym(\mathcal{L}, \mathcal{L})$ such that

$$F = RU \;\; \Rightarrow \;\; F^i_A = R^i_B U^B_A \tag{5}$$

and

$$U^B_A = \left(R^{-1}\right)^B_i F^i_A = \left(R^T\right)^B_i F^i_A \tag{6}$$

The tensors R and U are named macrorotation tensor and strain tensor, respectively. The difference between the Cauchy-Green tensor $C = F^T F$ and the identity matrix I gives the first deformation measure $E = \frac{1}{2}(F^T F - I)$. It is usually called Green–Saint–Venant tensor (or nonlinear macro-strain), and in components, it has the expression

$$E_{MN} = \frac{1}{2}(C_{MN} - \delta_{MN}) = \frac{1}{2}\left[G_{NA}\left(F^T\right)^A_b F^b_M - \delta_{MN}\right] = \frac{1}{2}(g_{ab} F^a_N F^b_M - \delta_{MN}) \tag{7}$$

where

$$\left(F^T\right)^A_b = G^{AC} F^a_C g_{ab} \tag{8}$$

The symbols G and g denote the Lagrangian and Eulerian metric tensor, respectively. Since E_A and e_i are orthonormal bases of the Lagrangian and Eulerian spaces, both are assumed equal to the Kronecker delta δ from now on.

2.1.2. Relative rotation tensor. The present paper aims to find a way to easily highlight the effect of micro/macro-relative rotations of a micropolar Cosserat continuum. The term microrotation refers to the particle rotation. Instead, we call macrorotation the rigid rotation of the infinitesimal portion of the continuum in the neighbourhoods of the considered particles. To this purpose, a new deformation tensor is identified. In the field of the Cosserat theory, many authors (see [68,69]) prefer to define the stretch tensor $\bar{\mathcal{E}}$ equal (except for constants) to $(\mathcal{C} - I)$, $\bar{\mathcal{E}} = \mathcal{C} - I$, where $\mathcal{C} = Q^T RU = Q^T F$ includes all the main physical quantities related to a Cosserat continuum: the tensors F, R and Q. Then, they usually introduce a deformation energy density as a function of the stretch tensor $\bar{\mathcal{E}}$ and of the wryness tensor $\varGamma$ (see Eq. (17)), $W^{\mathrm{def}}(\bar{\mathcal{E}}, \varGamma)$. Albeit $\bar{\mathcal{E}}$ and $\varGamma$ are enough to completely describe the kinematic behaviours of a micropolar continuum, this kind of procedure leads to a deformation energy density which does not clearly separate classic and non-classic energetic contributions. On the contrary, to consider the deformation energy density, $W^{\mathrm{def}}(E, \mathcal{R}, \varGamma)$, as a function of the Green–Saint–Venant tensor E (see Eq. (7)), the relative rotation tensor $\mathcal{R}$, (that we are going to introduce) and the wryness tensor $\varGamma$ allow to emphasize the effects due to the stretch, the micro/macro-relative rotation and the spatial variability of the microrotations. The author's subsequent proposal is the result of several attempts which will be summarized below.

Firstly, the tensor $Q^T R - I$ has been studied: it is objective (in the sense clarified in Sect. 2.2); it depends entirely on R and Q and, as a consequence, it would seem the perfect choice to take into account the micro/macro-relative rotation. Nevertheless, it is complicated to implement in a finite element code due to the structure of R, given by

$$R = FU^{-1} = F\left(F^T F\right)^{-\frac{1}{2}} \tag{9}$$

Equation (9) shows that R is a function of a square root of a matrix which is not easy to determine in a symbolic way. The author also tried to run numerical simulations where a positive definite deformation energy density was considered dependent on $Q^T R - I$. The software COMSOL Multiphysics® has been used, and convergence difficulties have been noted. The latter are related to the structure of R, whose analytical expression as a function of displacements is not known a priori, and whose computation requires finding eigenvalues and eigenvectors of the matrix $F^T F$. Interesting studies on the topic by Zubov and Rudev [70] and Bouby et al. [71] try to evaluate directly the square root of a matrix and the macrorotation matrix R; however, they do not seem very comfortable for numerical evaluations by means of a commercial finite element software. This paper aims to find a relative rotation tensor that results immediately applicable and symbolically defined.

Secondly, the difference $Q - R$ would seem another suitable choice. It is common in 2D problems the definition of the difference between the two representative angles of the macro- and microrotation. Unfortunately, the aforementioned tensor is clearly non-objective.

In light of all the above remarks, the author chooses to overcome all the listed problems and to introduce the new relative rotation tensor $\mathcal{R}$ as

$$\mathcal{R} = \frac{1}{2}\left[\left(Q^T F\right)^2 - \left(R^T F\right)^2\right] = \frac{1}{2}\left[\left(Q^T F\right)^2 - C\right] \tag{10}$$

which in components becomes

$$\mathcal{R}_{MN} = \frac{1}{2}\left[G_{AN}\left(Q^T\right)^A_i F^i_L \left(Q^T\right)^L_j F^j_M - C_{MN}\right] \tag{11}$$

The tensor $\mathcal{R}$ is objective (see Sect. 2.2); it is equal to zero if R is equal to Q; it does not need the computation of square roots of matrices and it is immediately implementable in a finite element software without all the computational difficulties related to the structure of R (see Eq. (9)). The Green–Saint–Venant tensor E and the relative rotation tensor $\mathcal{R}$ are not independent. It is not difficult to verify that $C = \left(\bar{\mathcal{E}} + I\right)^T \left(\bar{\mathcal{E}} + I\right)$, $E = 1/2\left[\bar{\mathcal{E}}^T \bar{\mathcal{E}} + \bar{\mathcal{E}}^T + \bar{\mathcal{E}}\right]$, and $\mathcal{R} = 1/2[\left(\bar{\mathcal{E}} + I\right)^2 - \left(\bar{\mathcal{E}} + I\right)^T \left(\bar{\mathcal{E}} + I\right)]$. If an approximately linear constitutive relationship is supposed with respect to both $\bar{\mathcal{E}}$ and R, the tensors E and $\mathcal{R}$ are reduced to the symmetric and the skewsymmetric part of $\bar{\mathcal{E}}$, respectively: $E \approx {}_S\bar{\mathcal{E}}$, $\mathcal{R} \approx {}_A\bar{\mathcal{E}}$, where ${}_S\bar{\mathcal{E}} = 1/2\left(\bar{\mathcal{E}} + \bar{\mathcal{E}}^T\right)$ and ${}_A\bar{\mathcal{E}} = 1/2\left(\bar{\mathcal{E}} - \bar{\mathcal{E}}^T\right)$. The previous statement can be easily justified thanks to the definition of $\mathcal{R}$. The Green–Saint–Venant tensor E and the relative rotation tensor $\mathcal{R}$ represent two different kinds of deformation measures. The first measures how much the distance between body particles changes after the motion, and the second measures the difference between micro- and macrorotations. If a continuum body is subjected to a rigid motion, the displacement gradient F is given by an orthogonal matrix O, $F = O$ and $O^T O = I$ is an identity matrix, then, $E = 0$ and $\mathcal{R} = 0$. Otherwise, if the body motion implies equals micro- and macrorotations, $Q = R$, then $E = 1/2(F^T F - I)$ and $\mathcal{R} = 0$, where $R = F\left(F^T F\right)^{-1/2} = Q$. Finally, if F is equal to an orthogonal matrix O, such that $F = O$, but the motion is not rigid with respect to both translation and rotation, $Q \neq O$, then, $E = 0$, $\mathcal{R} = 1/2[\left(Q^T O\right)^2 - I]$.

In the field of the linearized theory, the tensors F, Q and R can be written as $F \approx I + \eta\nabla\tilde{u} = I + \eta\tilde{H}$, where $\nabla\tilde{u} = \tilde{H}$ (see Bichara and dell'Isola [72]), $Q \approx I + \eta\tilde{Q}$ and $R \approx I + \eta\tilde{R}$ by neglecting each term of the order of $O\left(\eta^2\right)$. If the last expressions are replaced into Eqs. (10, 11), we obtain that $\mathcal{R} \approx \eta\tilde{Q}^T - \eta\tilde{R}^T \approx Q^T - R^T$. Since in the field of the linearized theory, the tensors R and Q are skewsymmetric, we have $R \approx I + {}_AR$ and $Q \approx I + {}_AQ$, where ${}_AR = \eta\tilde{R}$ and ${}_AQ = \eta\tilde{Q}$. Then, the relative rotation tensor $\mathcal{R}$ becomes approximately equal to the difference between ${}_AR$ and ${}_AQ$: $\mathcal{R} \approx {}_AR - {}_AQ \approx {}_A\nabla u - {}_AQ$, where ${}_A\nabla u$ is the skewsymmetric part of the matrix ∇u.

It could be interesting to notice that a link between the relative rotation here exposed and the one introduced by Misra et al. [73] is conceivable. Misra et al. [73] define, in the field of the macromorphic theory, the relative micro/macro-Green–Saint–Venant tensor $\varUpsilon$ equal to $1/2\left(I - \mathcal{P}^T \mathcal{F}^{-T}\right)$, in which $\mathcal{F} = \nabla_X \chi$, χ is the placement function of the grain of each sub-body, $\mathcal{P} = \nabla_X \chi'$, χ' is the placement function of each other point of the sub-body. If the relative rotation $\mathcal{R}$ (see Eq. (10)) is assumed to be equal to Υ, then, the tensor $\mathcal{P}$ becomes equal to $F\left(-\mathcal{R}^T+I\right)$. In this way, a possible relationship between $\mathcal{P}$, Q and F is derived, and a link between the micropolar and micromorphic theories is created. Of course, this is not the only possible alternative.

2.1.3. Wryness tensor. The last deformation measure linked to the gradient of Q is recalled. Let us consider the orthogonal structure of Q which implies the equality

$$\left(Q^T\right)_i^B Q_A^i=\delta_A^B \tag{12}$$

The derivation of each member of Eq. (12) with respect to X^C allows to prove the skewsymmetric structure of the application $\nabla Q^T Q$, which in components can be expressed as

$$\left(Q^T\right)_{i,C}^B Q_A^i=-\left(Q^T\right)_i^B Q_{A,C}^i \tag{13}$$

Although the tensor $\nabla Q^T Q$ is objective and it could be taken as the wryness tensor, it is a third-order tensor that is difficult to manipulate.

The skewsymmetric structure of $\nabla Q^T Q$ expressed by Eq. (13) implies, however chosen the index C, the existence of an axial vector. Then, the known wryness tensor Γ can be defined by

$$\left(Q^T\right)_{i,C}^A Q_M^i=-\left(Q^T\right)_i^A Q_{M,C}^i=\epsilon_{BM}{}^A\Gamma_C^B \tag{14}$$

where $\epsilon_{BM}{}^A$ is the Levi–Civita indicator. If the indicator $\epsilon^{LM}{}_A$ is defined such that

$$\epsilon_{BM}{}^A\epsilon^{LM}{}_A=2\delta_B^L \tag{15}$$

and if each member of Eq. (14) is multiplied by the indicator $\epsilon^{LM}{}_A$, we arrive to

$$\frac{1}{2}\epsilon^{LM}{}_A\left(Q^T\right)_{i,C}^A Q_M^i=-\frac{1}{2}\epsilon^{LM}{}_A\left(Q^T\right)_i^A Q_{M,C}^i=\delta_B^L\Gamma_C^B=\Gamma_C^L \tag{16}$$

Throughout the whole paper, the tensor Γ is supposed to be a covariant tensor:

$$\Gamma_{MN}=\frac{1}{2}G_{LM}\epsilon^{LC}{}_A\left(Q^T\right)_{i,N}^A Q_C^i \tag{17}$$

The choice of Γ was motivated by [68]; moreover, the author chose to consider it as a covariant tensor in analogy with the Cauchy-Green and relative rotation tensors.

2.1.4. Microrotation test function. In addition to introduce a new relative rotation tensor and to provide a micropolar theory by means of the Levi–Civita notation, the present paper aims to derive the Euler–Lagrange equations without considering Euler angles or by applying the Lagrange multiplier theorem. To this purpose, let us consider the equality

$$\left(Q^T\right)_i^B Q_A^i=\delta_A^B \tag{18}$$

If the variation of each member of Eq. (18) is evaluated, it is obtained

$$\delta\left(Q^T\right)_i^B Q_A^i=-\left(Q^T\right)_i^B\delta Q_A^i \tag{19}$$

Since Eq. (19) implies the skewsymmetric structure of $\delta Q^T Q$, it is allowed to define the vector function $\delta\omega$ such that

$$\delta\left(Q^T\right)_i^A Q_M^i=-\left(Q^T\right)_i^A\delta Q_M^i=\epsilon_{jM}{}^A\delta\omega^j \tag{20}$$

We choose to name $\delta\omega$ "microrotation test function" and to derive the other two useful relations

$$\delta\left(Q^T\right)_i^A=\left(Q^T\right)_i^M\epsilon_{jM}{}^A\delta\omega^j \tag{21}$$

$$\delta Q_M^i=-Q_A^i\epsilon_{jM}{}^A\delta\omega^j \tag{22}$$

Equations (21) and (22) are particularly comfortable to perform the subsequent analytical steps and to couple the equilibrium equations.

2.2. Objectivity of deformation tensors

Let us call objectivity the property of invariance under the change of an observer in the Eulerian configuration (see [15]). It is an abuse of nomenclature since, more strictly, we should call objective a mathematical object that verifies the so-called principle of frame indifference (or principle of objectivity) (see [68,74]). The last principle collects three independent postulates: the principle of invariance under Euclidean transformations, the principle of invariance under superposed rigid-body motions, and the principle of frame-invariance of the constitutive equations under change of observer. The property of invariance under a rigid motion in the current configuration is a necessary condition so that a tensor could represent an adequate measure of deformation. Let us consider the placement field in the infinitesimal neighbourhood of a fixed point X_0, which can be written as

$$\chi_t^i(X) - \chi_t^i(X_0) = \left.\frac{\partial \chi_t^i}{\partial X^A}\right|_{X_0} \left(X^A - X_0^A\right) = \left.F_A^i\right|_{X_0} \left(X^A - X_0^A\right) \tag{23}$$

Equation (23) implies the study of only local deformations (which is enough since the Principle of Local Action is implicitly postulated throughout the article) and it does not add any hypothesis about the displacement amplitude. Let us fix another instant t^* in which the images of the placement field differ from the ones in the instant t due to a rigid act of motion. Then, we have

$$\chi_{t^*}^j(X) - \chi_{t^*}^j(X_0) = O_i^j \left[\chi_t^i(X) - \chi_t^i(X_0)\right] \tag{24}$$

where $O \in Ort(\mathcal{E}, \mathcal{E})$. Since it is true the following equality

$$\chi_{t^*}^j(X) - \chi_{t^*}^j(X_0) = \left.\frac{\partial \chi_{t^*}^j}{\partial X^A}\right|_{X_0} \left(X^A - X_0^A\right) = \left.(F^*)_A^j\right|_{X_0} \left(X^A - X_0^A\right) \tag{25}$$

the link between the placement gradient in the instant t, F, and t^*, F^* is

$$(F^*)_A^j = O_i^j F_A^i \tag{26}$$

that in matrix form becomes

$$F^* = OF \tag{27}$$

Equation (26) shows the potential of the Levi–Civita notation: the presence of small letters as indices of O confirms that the rigid motion is fixed inside the Eulerian space. A similar reasoning is applied for deriving the relationship between the microrotation tensor in the instant t, Q, and t^*, Q^*. We get

$$(e')_{j'}^* = Q^* E'_{B'} \delta_{j'}^{B'} = O e'_{j'} = OQ E'_{B'} \delta_{j'}^{B'} \tag{28}$$

then

$$Q^* = OQ \tag{29}$$

Finally, the polar decomposition theorem is taken into account with the aim of deriving the useful relationship between R (in the instant t) and R^* (in the instant t^*) which can be expressed as

$$R^* = F^* \left[(F^*)^T F^*\right]^{-1/2} = OF \left(F^T O^T O F\right)^{-1/2} = OR \tag{30}$$

If the configurations in t^* and t differ only because of a rigid motion, the deformation energies of the system in t^* and t need to be equal. We say that the deformation tensors must be objective, i.e. invariant in t and t^*. The Green–Saint–Venant tensor E, the new relative rotation tensor $\mathcal{R}$ presented here and the wryness tensor Γ satisfy the previous property as proved below. We have

$$E^* = \frac{1}{2}(C^* - I) = \frac{1}{2}\left[(F^*)^T F^* - I\right] = \frac{1}{2}(F^T O^T O F - I) = \frac{1}{2}(F^T F - I) = E \tag{31}$$

$$2\mathcal{R}^* = (Q^*)^T (F^*) (Q^*)^T (F^*) - (C^*) = Q^T O^T O F Q^T O^T O F - C = \left(Q^T F\right)^2 - C = 2\mathcal{R} \tag{32}$$

and

$$\frac{1}{2}G_{LM}\epsilon^{LC}{}_{A}\left(\left(Q^{*}\right)^{T}\right)^{A}_{i,N}\left(Q^{*}\right)^{i}_{C}=\frac{1}{2}G_{LM}\epsilon^{LC}{}_{A}\left(Q^{T}\right)^{A}_{j,N}\left(O^{T}\right)^{j}_{i}O^{i}_{k}\left(Q\right)^{k}_{C}=\frac{1}{2}G_{LM}\epsilon^{LC}{}_{A}\left(Q^{T}\right)^{A}_{i,N}\left(Q\right)^{i}_{C} \tag{33}$$

which implies $\mathit{\Gamma}^{*}=\mathit{\Gamma}$.

3. Action functional

In this section, the same arguments developed by Auffrey et al. [15], for founding second gradient continuum mechanics, are exploited to found nonlinear micropolar continuum mechanics. The Levi–Civita absolute tensor calculus is extensively used.

Let us introduce the following action functional

$$\mathcal{A}=\int_{t_0}^{t_1}\int_{\mathcal{L}}\left[\frac{1}{2}\rho_0 v\cdot v+\frac{1}{2}I_0\Theta\cdot\Theta-W\left(\chi,Q,E,\mathcal{R},\mathit{\Gamma},X\right)\right]\mathrm{d}V\mathrm{d}t+\int_{t_0}^{t_1}\int_{\partial\mathcal{L}}\left[-W_S\left(\chi,Q,X\right)\right]\mathrm{d}A\mathrm{d}t \tag{34}$$

where

- the field χ denotes the placement field between $\mathcal{L}$ and $\mathcal{E}$
$$\chi:\mathcal{L}\to\mathcal{E} \tag{35}$$
- the fields $\rho_0\left(X\right)$ and $I_0\left(X\right)$ refer to the Lagrangian time-independent mass density and to the Lagrangian time-independent proper spin of material points;
- the symbols E, $\mathcal{R}$ and $\mathit{\Gamma}$ represent the Green–Saint–Venant tensor, the relative rotation tensor and the wryness tensor, respectively (see Eqs. (7-11-17));
- $v=\frac{\partial\chi}{\partial t}$ and $\Theta=\frac{\partial Q}{\partial t}$ are the Lagrangian translational and rotational velocities;
- the product $v\cdot v$ and $\Theta\cdot\Theta$ are equal to $v_b v^b=g_{ab}v^a v^b$ and $\Theta^i_A\Theta^A_i=g_{ik}\Theta^k_B\Theta^i_A G^{BA}$;
- the potential $W\left(\chi,Q,E,\mathcal{R},\mathit{\Gamma},X\right)$ is relative to the volumic density of action inside the volume $\mathcal{L}$;
- the potential $W_S\left(\chi,Q,X\right)$ is relative to the actions externally applied at the boundary $\partial\mathcal{L}$.

The internal energy W can be split into two addends: the objective deformation energy density W^{def} (see Eqs. (31–33)) and an external conservative action of a bulk load $\mathcal{U}^{\mathrm{ext}}$

$$W\left(\chi,Q,E,\mathcal{R},\mathit{\Gamma},X\right)=W^{\mathrm{def}}\left(E,\mathcal{R},\mathit{\Gamma},X\right)+\mathcal{U}^{\mathrm{ext}}\left(\chi,Q,X\right) \tag{36}$$

The first variation of the part of the action functional related to the deformation energy can be written as the sum of three terms

$$\delta\mathcal{A}^{\mathrm{def}}=\delta\mathcal{A}^{\mathrm{def}}_{E}+\delta\mathcal{A}^{\mathrm{def}}_{\mathcal{R}}+\delta\mathcal{A}^{\mathrm{def}}_{\mathit{\Gamma}} \tag{37}$$

In detail, we have:

$$\delta\mathcal{A}^{\mathrm{def}}_{E}=-\int_{t_0}^{t_1}\int_{\mathcal{L}}\frac{\partial W^{\mathrm{def}}}{\partial E_{MN}}\delta E_{MN}\mathrm{d}V\mathrm{d}t \tag{38}$$

$$\delta\mathcal{A}^{\mathrm{def}}_{\mathcal{R}}=-\int_{t_0}^{t_1}\int_{\mathcal{L}}\frac{\partial W^{\mathrm{def}}}{\partial \mathcal{R}_{MN}}\delta \mathcal{R}_{MN}\mathrm{d}V\mathrm{d}t \tag{39}$$

$$\delta\mathcal{A}^{\mathrm{def}}_{\mathit{\Gamma}}=-\int_{t_0}^{t_1}\int_{\mathcal{L}}\frac{\partial W^{\mathrm{def}}}{\partial \mathit{\Gamma}_{MN}}\delta \mathit{\Gamma}_{MN}\mathrm{d}V\mathrm{d}t \tag{40}$$

3.1. Piola stress tensor

To introduce the Piola stress tensor, we need to compute the first variation $\delta\mathcal{A}_E^{\mathrm{def}}$ (38). Definition (7) of the Green–Saint–Venant tensor allows to write

$$\delta E_{MN} = \frac{1}{2}\delta C_{MN} = \frac{1}{2}(g_{ab}\delta F_N^a F_M^b + g_{ab}F_N^a \delta F_M^b) \tag{41}$$

If Eq. (41) is replaced into Eq. (38), by taking into account the symmetry of E and integrating one time by parts, we get

$$\delta\mathcal{A}_E^{\mathrm{def}} = -\int_{t_0}^{t_1}\int_{\partial\mathcal{L}}\left(\frac{\partial W^{\mathrm{def}}}{\partial E_{MN}}F_N^a g_{ab}\right)N_M\delta\chi^b \mathrm{d}A\mathrm{d}t + \int_{t_0}^{t_1}\int_{\mathcal{L}}\frac{\partial}{\partial X^M}\left(\frac{\partial W^{\mathrm{def}}}{\partial E_{MN}}F_N^a g_{ab}\right)\delta\chi^b \mathrm{d}V\mathrm{d}t. \tag{42}$$

Since the Piola stress tensor can be defined by

$$\mathbb{P}_b^M = \frac{\partial W^{\mathrm{def}}}{\partial E_{MN}}F_N^a g_{ab} = 2\frac{\partial W^{\mathrm{def}}}{\partial C_{MN}}F_N^a g_{ab}, \tag{43}$$

the expression (42) becomes

$$\delta\mathcal{A}_E^{\mathrm{def}} = -\int_{t_0}^{t_1}\int_{\partial\mathcal{L}}\mathbb{P}_b^M N_M\delta\chi^b \mathrm{d}A\mathrm{d}t + \int_{t_0}^{t_1}\int_{\mathcal{L}}\frac{\partial}{\partial X^M}\left(\mathbb{P}_b^M\right)\delta\chi^b \mathrm{d}V\mathrm{d}t \tag{44}$$

3.2. Piola-type micropolar stress tensor

The present subsection aims to evaluate the first variation $\delta\mathcal{A}_{\mathcal{R}}^{\mathrm{def}}$(39). Definition (11) of the relative rotation tensor allows to write

$$\delta\mathcal{R}_{MN} = \frac{1}{2}\left[G_{NA}\delta\left(Q^T F\right)_L^A\left(Q^T F\right)_M^L + G_{NA}\left(Q^T F\right)_L^A\delta\left(Q^T F\right)_M^L - \delta C_{MN}\right] \tag{45}$$

If Eqs. (21) and (7) are taken into account, Eq. (45) allows to achieve

$$\frac{\partial W^{\mathrm{def}}}{\partial\mathcal{R}_{MN}}\delta\mathcal{R}_{MN} = \mathbb{V}_j^{(\mathrm{I})}\delta\omega^j + \left[\mathbb{F}_b^{M(\mathrm{I})} + \mathbb{F}_b^{M(\mathrm{II})}\right]\delta F_M^b \tag{46}$$

where

$$\mathbb{F}_b^{M(\mathrm{I})} = \frac{1}{2}\left[\frac{\partial W^{\mathrm{def}}}{\partial\mathcal{R}_{MN}}\left(Q^T\right)_i^A\left(Q^T\right)_b^B + \frac{\partial W^{\mathrm{def}}}{\partial\mathcal{R}_{BN}}\left(Q^T\right)_b^A\left(Q^T\right)_i^M\right]G_{AN}F_B^i \tag{47}$$

$$\mathbb{F}_b^{M(\mathrm{II})} = -\frac{1}{2}\left(\frac{\partial W^{\mathrm{def}}}{\partial\mathcal{R}_{MN}} + \frac{\partial W^{\mathrm{def}}}{\partial\mathcal{R}_{NM}}\right)g_{ab}F_N^a \tag{48}$$

$$\mathbb{V}_j^{(\mathrm{I})} = \frac{1}{2}\frac{\partial W^{\mathrm{def}}}{\partial\mathcal{R}_{MN}}\epsilon_{jD}{}^B\left[G_{BN}F_A^k F_M^i + G_{AN}F_B^i F_M^k\right]\left(Q^T\right)_i^A\left(Q^T\right)_k^D \tag{49}$$

If Eqs. (46–49) are replaced into Eq. (39) and if the latter is integrated one time by parts, the first variation $\delta\mathcal{A}_{\mathcal{R}}^{\mathrm{def}}$ becomes

$$\delta\mathcal{A}_{\mathcal{R}}^{\mathrm{def}} = -\int_{t_0}^{t_1}\int_{\mathcal{L}}\mathbb{V}_j^{(\mathrm{I})}\delta\omega^j \mathrm{d}V\mathrm{d}t - \int_{t_0}^{t_1}\int_{\partial\mathcal{L}}\mathbb{F}_b^M N_M\delta\chi^b \mathrm{d}A\mathrm{d}t + \int_{t_0}^{t_1}\int_{\mathcal{L}}\frac{\partial}{\partial X^M}\left(\mathbb{F}_b^M\right)\delta\chi^b \mathrm{d}V\mathrm{d}t \tag{50}$$

where the new tensor $\mathbb{F}$ is named "Piola-type micropolar stress tensor" by the author and it is defined as $\mathbb{F} = \mathbb{F}^{(\mathrm{I})} + \mathbb{F}^{(\mathrm{II})}$; the new vector $\mathbb{V}^{(\mathrm{I})}$ is called "first Lagrangian stress vector". Both have been derived here for the first time.

3.3. Piola-type couple stress tensor

To introduce such tensor, it is necessary to compute the first variation $\delta\mathcal{A}_{\Gamma}^{\mathrm{def}}$ (37). Definition (17) of the wryness tensor allows to write

$$\delta\Gamma_{MN} = \frac{1}{2}G_{LM}\epsilon^{LC}{}_{A}\delta\left(Q^{T}\right)^{A}_{i,N}Q^{i}_{C} + \frac{1}{2}G_{LM}\epsilon^{LC}{}_{A}\left(Q^{T}\right)^{A}_{i,N}\delta Q^{i}_{C} \tag{51}$$

Equation (21) leads to

$$\delta\left(Q^{T}\right)^{A}_{i,N} = \left(Q^{T}\right)^{D}_{i,N}\epsilon_{jD}{}^{A}\delta\omega^{j} + \left(Q^{T}\right)^{D}_{i}\epsilon_{jD}{}^{A}\delta\omega^{j}_{,N} \tag{52}$$

If Eqs. (52-22) are replaced into Eq. (51), then

$$\delta\Gamma_{MN} = \frac{1}{2}G_{LM}\left(\epsilon^{LC}{}_{A}\epsilon_{jD}{}^{A} - \epsilon^{LA}{}_{D}\epsilon_{jA}{}^{C}\right)\left(Q^{T}\right)^{D}_{i,N}Q^{i}_{C}\delta\omega^{j} + G_{LM}\delta^{L}_{j}\delta\omega^{j}_{,N} \tag{53}$$

If Eq. (53) is replaced into Eq. (40), we arrive to

$$\delta\mathcal{A}_{\Gamma}^{\mathrm{def}} = -\int_{t_0}^{t_1}\int_{\mathcal{L}}\left[\frac{1}{2}\frac{\partial W^{\mathrm{def}}}{\partial\Gamma_{MN}}G_{LM}\left(\epsilon^{LC}{}_{A}\epsilon_{jD}{}^{A} - \epsilon^{LA}{}_{D}\epsilon_{jA}{}^{C}\right)\left(Q^{T}\right)^{D}_{i,N}Q^{i}_{C}\delta\omega^{j} + G_{LM}\frac{\partial W^{\mathrm{def}}}{\partial\Gamma_{MN}}\delta^{L}_{j}\delta\omega^{j}_{,N}\right]\mathrm{d}V\mathrm{d}t \tag{54}$$

The tensor $\mathbb{M}$ and the vector $\mathbb{V}^{(\mathrm{II})}$ that the author chooses to name “Piola-type couple stress tensor” and “second Lagrangian stress vector” are defined as

$$\mathbb{M}^{N}_{j} = G_{LM}\frac{\partial W^{\mathrm{def}}}{\partial\Gamma_{MN}}\delta^{L}_{j} = G_{jM}\frac{\partial W^{\mathrm{def}}}{\partial\Gamma_{MN}} \tag{55}$$

$$\mathbb{V}^{(\mathrm{II})}_{j} = \frac{1}{2}\frac{\partial W^{\mathrm{def}}}{\partial\Gamma_{MN}}G_{LM}\left(\epsilon^{LC}{}_{A}\epsilon_{jD}{}^{A} - \epsilon^{LA}{}_{D}\epsilon_{jA}{}^{C}\right)\left(Q^{T}\right)^{D}_{i,N}Q^{i}_{C} \tag{56}$$

Finally, positions (55), (56) and one integration by parts lead to

$$\delta\mathcal{A}_{\Gamma}^{\mathrm{def}} = -\int_{t_0}^{t_1}\int_{\mathcal{L}}\mathbb{V}^{(\mathrm{II})}_{j}\delta\omega^{j}\mathrm{d}V\mathrm{d}t - \int_{t_0}^{t_1}\int_{\partial\mathcal{L}}\mathbb{M}^{N}_{j}N_{N}\delta\omega^{j}\mathrm{d}A\mathrm{d}t + \int_{t_0}^{t_1}\int_{\mathcal{L}}\frac{\partial}{\partial X^{N}}\left(\mathbb{M}^{N}_{j}\right)\delta\omega^{j}\mathrm{d}V\mathrm{d}t \tag{57}$$

Although the tensor $\mathbb{M}$ and the vector $\mathbb{V}^{(\mathrm{II})}$ have been derived within well-known kinematic hypotheses and they appear in the literature in different forms, the expressions proposed in Eq. (55) and (56) cannot be found according to the author’s knowledge.

3.4. Euler–Lagrange equations

The first variation linked to the external volume actions, $\delta\mathcal{A}^{\mathrm{ext}}$, gives

$$\delta\mathcal{A}^{\mathrm{ext}} = \int_{t_0}^{t_1}\int_{\mathcal{L}}T_{b}\delta\chi^{b}\mathrm{d}V\mathrm{d}t + \int_{t_0}^{t_1}\int_{\mathcal{L}}C_{j}\delta\omega^{j}\mathrm{d}V\mathrm{d}t \tag{58}$$

where the functions T_b and C_j are fixed equal to

$$T_{b} = -\frac{\partial\mathcal{U}^{\mathrm{ext}}}{\partial\chi^{b}} \tag{59}$$

$$C_{j} = \frac{\partial\mathcal{U}^{\mathrm{ext}}}{\partial Q^{i}_{M}}Q^{i}_{A}\epsilon_{jM}{}^{A} \tag{60}$$

On the other hand, the first variation linked to the surface actions, $\delta\mathcal{A}_S$, gives

$$\delta\mathcal{A}_S = \int_{t_0}^{t_1}\int_{\partial\mathcal{L}} t_b\delta\chi^b \mathrm{d}V\mathrm{d}t + \int_{t_0}^{t_1}\int_{\partial\mathcal{L}} c_j\delta\omega^j \mathrm{d}V\mathrm{d}t \tag{61}$$

in which the functions t_b and c_j are defined by

$$t_b = -\frac{\partial W_S}{\partial\chi^b} \tag{62}$$

$$c_j = \frac{\partial W_S}{\partial Q^i_M} Q^i_A \epsilon_{jM}{}^A \tag{63}$$

About the kinetic energy, it is interesting to show that its first variation, $\delta\mathcal{A}^{\mathrm{kin}}$, can be written in the form

$$\delta\mathcal{A}^{\mathrm{kin}} = \int_{\mathcal{L}} \left[\rho_0 v_b\delta\chi^b + I_0\vartheta_j\delta\omega^j\right]_{t_0}^{t_1} dV - \int_{t_0}^{t_1}\int_{\mathcal{L}} \left[\rho_0\frac{\partial v_b}{\partial t}\delta\chi^b + I_0\left(\frac{\partial\vartheta_j}{\partial t} + \psi_j\right)\delta\omega^j\right]\mathrm{d}V\mathrm{d}t \tag{64}$$

where ϑ_j and ψ_j are fixed equal to

$$\vartheta_j = -g_{ik}G^{BM}\Theta^k_B Q^i_A \epsilon_{jM}{}^A \tag{65}$$

$$\psi_j = g_{ik}G^{BM}\Theta^k_B \Theta^i_A \epsilon_{jM}{}^A \tag{66}$$

Since ψ_j gives zero if $g_{ik} = \delta_{ik}$ and $G^{BM} = \delta^{BM}$, the residual part $\partial\vartheta_j/\partial t$ needs to be the material inertial acceleration.

Equations (44-50-57) allow to evaluate the first variation linked to the deformation energy, $\delta\mathcal{A}^{\mathrm{def}}$. Now, the first variation of the full action functional, $\delta\mathcal{A}$, can be fixed equal to zero so as to derive the minimum of the action functional itself, which means to impose the equality

$$\delta\mathcal{A} = \delta\mathcal{A}^{\mathrm{kin}} + \delta\mathcal{A}^{\mathrm{def}} + \delta\mathcal{A}^{\mathrm{ext}} + \delta\mathcal{A}_S = 0 \tag{67}$$

Equation (67) leads to the Euler–Lagrangian equations for the nonlinear micropolar continuum:

- on the volume $\mathcal{L}$

$$-\rho_0\frac{\partial v_b}{\partial t} + \frac{\partial}{\partial X^M}\left(\mathbb{L}^M_b\right) + T_b = 0 \tag{68}$$

$$-I_0\frac{\partial\vartheta_j}{\partial t} + \frac{\partial}{\partial X^N}\left(\mathbb{M}^N_j\right) - \mathbb{V}_j + C_j = 0 \tag{69}$$

  where the new vector $\mathbb{V} = \mathbb{V}^{(\mathrm{I})} + \mathbb{V}^{(\mathrm{II})}$ (see Eqs. (49-56)) and the new tensor $\mathbb{L}$=$\mathbb{P}$+$\mathbb{F}$ (see Eqs. (43-47-48)) are named by the author "Lagrangian stress vector" and "Piola-type micropolar complete stress tensor"; $\mathbb{M}$ is the Piola-type couple stress tensor (see Eq. (55));
- on the boundary $\partial\mathcal{L}$

$$-\mathbb{L}^M_b N_M + t_b = 0 \tag{70}$$

$$-\mathbb{M}^N_j N_N + c_j = 0 \tag{71}$$

All the derived expressions are functions of the microrotation tensor Q. The microrotation test function $\delta\omega$ is mainly defined to couple the equilibrium equations and to avoid the application of the Lagrange multiplier theorem. Equations (70) and (71) describe how the sub-bodies of a given continuous body interact with each other in the field of the micropolar model here introduced: the sub-bodies shall exchange

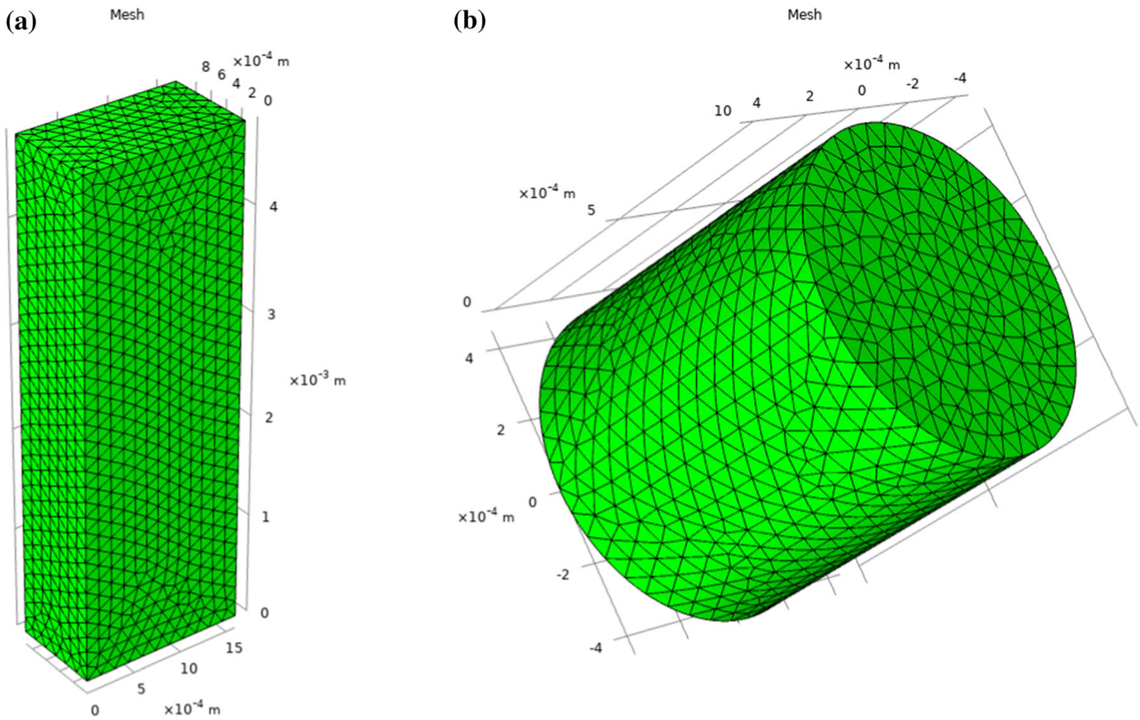

Fig. 2. Applied mesh for **a** axial and bending **b** torsion numerical tests

forces per unite area, $\mathbb{L}_b^M$, and couples per unite area, $\mathbb{M}_j^N$; moreover, in each infinitesimal volume of the continuum, couples of forces per unite area, $\mathbb{V}_j$, act (see Eq. (69)).

4. Numerical applications

In this section, several numerical applications are performed (without any kind of kinematic linearization) to investigate the effect of the new relative rotation tensor $\mathcal{R}$ (see Eqs. (10-11)) in the analysis of small elements and the ability of $\mathcal{R}$ to describe non-classic mechanical behaviours in the nonlinear field. The typical elements of a pantographic sheet are studied by means of axial, bending and torsion numerical tests. The choice to analyse the substructures of a pantographic sheet is motivated by two main reasons: the growing importance of pantographic structures within the scientific panorama; the dimensions of their substructures, beams and pivots, which result significantly small with respect to the media usually described by classical models. It is precisely the description of small samples together with granular and metamaterials that justifies the development of micropolar and second gradient theories. The numerical analyses are based on standard energy minimization techniques through the application of the standard finite element method (FEM) packages in COMSOL Multiphysics®. The geometrical characteristics and the boundary conditions will be specified individually for each case. Regarding the accuracy of the analyses, a free tetrahedral mesh with 33072 domain elements, 2944 boundary elements, and 196 edge elements is chosen for the axial and bending numerical tests (see Fig. 2a); 30947 domain elements, 2206 boundary elements, and 140 edge elements is chosen for the torsion numerical tests (see Fig. 2b). In both cases, quadratic Lagrange interpolating polynomials have been considered for all the kinematic unknowns of the differential problem.

4.1. Deformation energy density

An isotropic deformation energy density, denoted by W^{def}, quadratic with respect to E, $\mathcal{R}$, Γ is imposed. The tensors E, $\mathcal{R}$, Γ have been defined in Sect. 2.1. We are naturally leaded to

$$\begin{aligned} W^{\mathrm{def}} = \frac{\lambda_E}{2} Tr\,[E]^2 + \mu_E \left\| {}_S E \right\|^2 + \frac{\lambda_{\mathcal{R}}}{2} Tr\,[\mathcal{R}]^2 + \mu_{\mathcal{R}} \left\| {}_S \mathcal{R} \right\|^2 + \xi_{\mathcal{R}} \left\| {}_A \mathcal{R} \right\|^2 \\ + \frac{\lambda_\Gamma}{2} Tr\,[\Gamma]^2 + \left(\frac{\mu_\Gamma + \xi_\Gamma}{2} \right) \left\| {}_S \Gamma \right\|^2 + \left(\frac{\mu_\Gamma - \xi_\Gamma}{2} \right) \left\| {}_A \Gamma \right\|^2 \end{aligned} \tag{72}$$

in which, the symbols $Tr\,(\cdot)$ and $\|\cdot\|$ stand for the trace and Euclidean norm of a considered tensor, respectively. If a linear constitutive behaviour with respect to $\bar{\mathcal{E}} = Q^T F - I$ (see Subsubsection 2.1.2) is also supposed, Eq. (72) can be further simplified. In this case, E and $\mathcal{R}$ are reduced to the symmetric and skewsymmetric parts of $\bar{\mathcal{E}}$: $E \approx {}_S\bar{\mathcal{E}}$ and $\mathcal{R} \approx {}_A\bar{\mathcal{E}}$; Eq. (72) becomes

$$\begin{aligned} W^{\mathrm{def}} \approx \bar{W}^{\mathrm{def}} = \frac{\lambda_E}{2} Tr\left[{}_S\bar{\mathcal{E}} \right]^2 + \mu_E \left\| {}_S\bar{\mathcal{E}} \right\|^2 + \xi_{\mathcal{R}} \left\| {}_A\bar{\mathcal{E}} \right\|^2 + \frac{\lambda_\Gamma}{2} Tr\,[\Gamma]^2 \\ + \left(\frac{\mu_\Gamma + \xi_\Gamma}{2} \right) \left\| {}_S \Gamma \right\|^2 + \left(\frac{\mu_\Gamma - \xi_\Gamma}{2} \right) \left\| {}_A \Gamma \right\|^2 \end{aligned} \tag{73}$$

Therefore, the definition of $\mathcal{R}$ implies that the skewsymmetric part of $\bar{\mathcal{E}}$, ${}_A\bar{\mathcal{E}}$, can be also chosen as a measure of the micro/macro-relative rotation under appropriate constitutive assumptions. Hereafter, it will be shown that both Eqs. (72) and (73) can be seen as the nonlinearized expressions of the linearized micropolar strain energy widely used in the literature. In the field of the linearized theory, the tensors F, R and Q can be approximated up by first degree polynomials in η, neglecting every term of the order $O\left(\eta^2\right)$: $F \approx I + \eta \nabla \tilde{u}$; $R \approx I + \eta \tilde{R} = I + {}_A R$; $Q \approx I + \eta \tilde{Q} = I + {}_A Q$ (see Subsection 2.1.2). Introducing the tensor $\bar{\varepsilon}$, defined as the difference between the displacement gradient ∇u and the skewsymmetric part of the microrotation tensor Q in the linearized case, $\bar{\varepsilon} = \nabla u - {}_A Q$, the linearized forms of the deformation tensors (7), (11) and (17) can be achieved. We have

$$E \approx {}_S\bar{\mathcal{E}} \approx {}_S\bar{\varepsilon} \quad \mathcal{R} \approx {}_A\bar{\mathcal{E}} \approx {}_A\bar{\varepsilon} \quad \Gamma \approx \frac{1}{2}\epsilon : \nabla Q^T = \frac{1}{2}\epsilon : \nabla {}_A Q^T = \bar{\mathfrak{k}} \tag{74}$$

where ${}_S\bar{\varepsilon}$ denotes the symmetric part of $\bar{\varepsilon}$; ${}_A\bar{\varepsilon}$ the skewsymmetric part of $\bar{\varepsilon}$; the micro-rotation tensor Q is skewsymmetric. If Eq. (74) is replaced into Eq. (72) or into Eq. (73), we get

$$\begin{aligned} W^{\mathrm{def}} \approx w^{\mathrm{def}} = \frac{\lambda_E}{2} Tr\left[{}_S\bar{\varepsilon} \right]^2 + \mu_E \left\| {}_S\bar{\varepsilon} \right\|^2 + \xi_{\mathcal{R}} \left\| {}_A\bar{\varepsilon} \right\|^2 + \frac{\lambda_\Gamma}{2} Tr\left[\bar{\mathfrak{k}} \right]^2 + \left(\frac{\mu_\Gamma + \xi_\Gamma}{2} \right) \left\| {}_S\bar{\mathfrak{k}} \right\|^2 \\ + \left(\frac{\mu_\Gamma - \xi_\Gamma}{2} \right) \left\| {}_A\bar{\mathfrak{k}} \right\|^2 \end{aligned} \tag{75}$$

In the literature, the linearized micropolar strain energy function, that we denote by w^{def}_{mp}, is often written as (see [75])

$$w^{\mathrm{def}}_{mp} = \frac{\lambda}{2} Tr\left[{}_S\bar{\varepsilon} \right]^2 + \mu \left\| {}_S\bar{\varepsilon} \right\|^2 + \mu_c \left\| {}_A\bar{\varepsilon} \right\|^2 + \frac{\alpha}{2} Tr\left[\bar{\mathfrak{k}} \right]^2 + \left(\frac{\gamma + \beta}{2} \right) \left\| {}_S\bar{\mathfrak{k}} \right\|^2 + \left(\frac{\gamma - \beta}{2} \right) \left\| {}_A\bar{\mathfrak{k}} \right\|^2 \tag{76}$$

A comparison between Eqs. (72), (75) and (76) allows to state that five of the parameters appearing in the present paper are exactly the same of the classic micropolar ones. In detail, it is derived

$$\lambda_E = \lambda \quad \mu_E = \mu \quad \xi_{\mathcal{R}} = \mu_c \quad \lambda_\Gamma = \alpha \quad \mu_\Gamma = \gamma \quad \xi_\Gamma = \beta \tag{77}$$

The mathematical expression of Eq. (72) implies the following: it is necessary and sufficient condition for the nonlinearized deformation energy density W^{def} to be nonnegative definite that

$$\begin{aligned} \mu_E \geqslant 0 \quad 3\lambda_E + 2\mu_E \geqslant 0 \quad 3\lambda_{\mathcal{R}} + 2\mu_{\mathcal{R}} \geqslant 0 \quad \mu_{\mathcal{R}} \geqslant 0 \quad \xi_{\mathcal{R}} \geqslant 0 \\ \mu_\Gamma + \xi_\Gamma \geqslant 0 \quad \mu_\Gamma - \xi_\Gamma \geqslant 0 \quad 3\lambda_\Gamma + (\mu_\Gamma + \xi_\Gamma) \geqslant 0 \end{aligned} \tag{78}$$

Table 1. *Material parameters supposed in the numerical tests*

	λ_E(MPa)	μ_E(MPa)	$\lambda_{\mathcal{R}}$(MPa)	$\mu_{\mathcal{R}}$(MPa)	$\xi_{\mathcal{R}}$(MPa)	λ_Γ(MN)	μ_Γ(MN)	ξ_Γ(MN)
Type 1	$2\cdot 10^4$	$5.6\cdot 10^{-1}$	1	1	0	$2\cdot 10^{11}$	$5\cdot 10^{11}$	$3\cdot 10^{11}$
Type 2	$2\cdot 10^4$	$5.6\cdot 10^{-1}$	1	1	$5\cdot 10^{-1}$	$2\cdot 10^{11}$	$5\cdot 10^{11}$	$3\cdot 10^{11}$
Type 3	$2\cdot 10^4$	$5.6\cdot 10^{-1}$	1	1	$5\cdot 10^{4}$	$2\cdot 10^{11}$	$5\cdot 10^{11}$	$3\cdot 10^{11}$
Type 4	$2\cdot 10^4$	$5.6\cdot 10^{-1}$	1	1	$5\cdot 10^{7}$	$2\cdot 10^{11}$	$5\cdot 10^{11}$	$3\cdot 10^{11}$

In the numerical application, the author considered the nonlinearized energetic model (72), W^{def}, whose nonnegativity is given by positions (78). The material constants λ_E and μ_E are the Lamé parameters. Indeed, different constitutive hypotheses could be made and internal energies of a bigger order could be considered: from a practical point of view, it is better to limit the number of constitutive moduli since the considerable difficulties related to their identification. The material parameters chosen for the numerical tests are listed in Table 1: since $\xi_{\mathcal{R}}$ leads to the most exotic results, four different values of $\xi_{\mathcal{R}}$ are fixed to understand its effect on the mechanical response of the samples. All the numerical applications have been performed without caring about the amplitude of displacements. This is possible thanks to the general definition of the deformation tensors (7), (11) and (17). On the contrary, Eqs. (75), (76) hold just for small displacements and rotations.

4.2. Axial test

Firstly, a simple rectangular beam of base $b = 0.9\,\text{mm}$, height $h = 1.6\,\text{mm}$ and length $l = 4.8\,\text{mm}$ is analysed. In the clamped section, both displacements and rotations are blocked. The boundary conditions are detailed below:

$$u^1\left(X^1,X^2,0\right) = u^2\left(X^1,X^2,0\right) = u^3\left(X^1,X^2,0\right) = 0 \tag{79}$$

$$Q^1_1\left(X^1,X^2,0\right) = Q^2_2\left(X^1,X^2,0\right) = 1 \quad Q^1_2\left(X^1,X^2,0\right) = Q^2_1\left(X^1,X^2,0\right) = 0 \tag{80}$$

$$u_3\left(X^1,X^2,l\right) = 1\cdot 10^{-3}\,\text{m} \tag{81}$$

Albeit Eq. (80) expresses the boundary conditions in terms of the entrances of the microrotation tensor Q, an alternative description is possible. The microrotation tensor Q can be directly defined in terms of three angles r^1, r^2 and r^3 , commonly known as Euler angles, which describe the rotations around the axes whose directions are defined by E_1, E_2 and E_3. A microrotation of r^1 radians around E_1 is given by

$$Q_{E_1} = \begin{bmatrix} 1 & 0 & 0 \\ 0 & \cos r^1 & -\sin r^1 \\ 0 & \sin r^1 & \cos r^1 \end{bmatrix} \tag{82}$$

In the same way, a microrotation of r^2 radians around E_2 is described by

$$Q_{E_2} = \begin{bmatrix} \cos r^2 & 0 & \sin r^2 \\ 0 & 1 & 0 \\ -\sin r^2 & 0 & \cos r^2 \end{bmatrix} \tag{83}$$

Finally, a microrotation of r^3 radians around E_3 is modelled by

$$Q_{E_3} = \begin{bmatrix} \cos r^3 & -\sin r^3 & 0 \\ \sin r^3 & \cos r^3 & 0 \\ 0 & 0 & 1 \end{bmatrix} \tag{84}$$

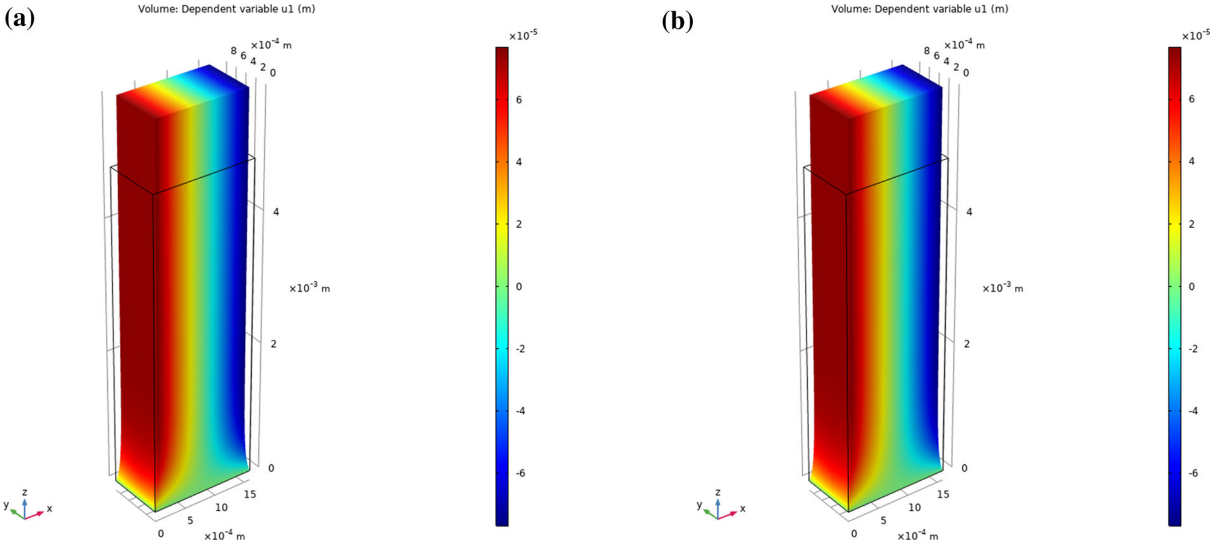

FIG. 3. Axial test: transversal displacement u_1 for material parameters of **a** Type 1 **b** Type 2

The general microrotation matrix Q can be expressed as the product between Q_{E_3}, Q_{E_2} and Q_{E_1} so as to obtain

$$Q = Q_{E_3} Q_{E_2} Q_{E_1} \tag{85}$$

that, in an explicit form, is equal to

$$Q = \begin{bmatrix} \cos r^2 \cos r^3 & \sin r^1 \sin r^2 \cos r^3 - \cos r^1 \sin r^3 & \cos r^1 \sin r^2 \cos r^3 + \sin r^1 \sin r^3 \\ \cos r^2 \sin r^3 & \sin r^1 \sin r^2 \sin r^3 + \cos r^1 \cos r^3 & \cos r^1 \sin r^2 \sin r^3 - \sin r^1 \cos r^3 \\ -\sin r^2 & \sin r^1 \cos r^2 & \cos r^1 \cos r^2 \end{bmatrix} \tag{86}$$

In view of this, Eq. (80) can be rewritten as

$$r^1 \left(X^1, X^2, 0 \right) = r^2 \left(X^1, X^2, 0 \right) = r^3 \left(X^1, X^2, 0 \right) = 0 \tag{87}$$

In summary, two procedures can be followed:

1 to define the microrotation tensor Q by adding the six constraints $Q^T Q = I$ and $det\,[Q] = 1$;
2 to define Q by means of the angles r^1, r^2 and r^3.

The second listed is preferred in this paper since it results advantageous from a computational point of view if statistical problems are faced and small microrotations appear; if not, there are some difficulties related to the periodic structures of the entrances of Q in Eq. (85). Another questionable aspect is the existence of different angles and rotation matrices able to describe the same 3D rigid rotation.

The displacements u_1, u_2 and u_3 that are obtained under the hypotheses of material parameters of Type 1, Type 2, Type 3 and Type 4 (see Table 1) are shown in Figs. 3, 4, 5, 6 and 7, 8. The presented set of figures show that the growth of the constitutive parameter $\xi_{\mathcal{R}}$ related to skewsymmetric part of the relative rotation tensor $\mathcal{R}$ progressively reduces the transversal displacements. Although the same axial displacements can be predicted also by classical elasticity, the possibility to predict transversal displacements progressively equal to zero is a peculiar aspect of the introduced model.

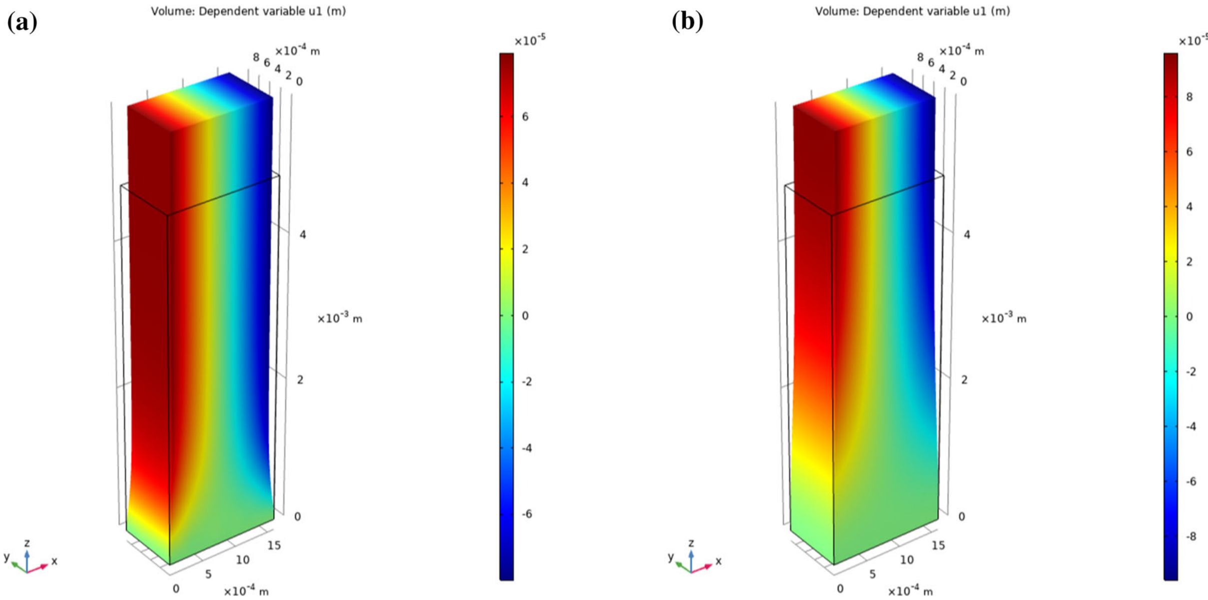

FIG. 4. Axial test: transversal displacement u_1 for material parameters of **a** Type 3 **b** Type 4

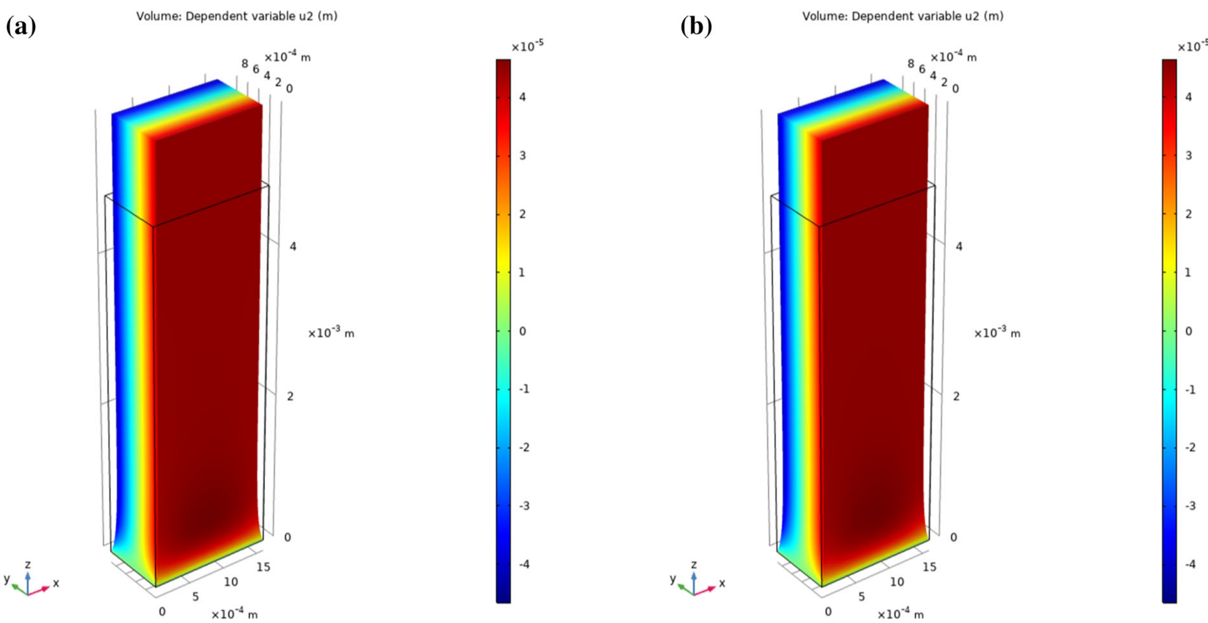

FIG. 5. Axial test: transversal displacement u_2 for material parameters of **a** Type 1 **b** Type 2

4.3. Bending test

The same beam as before is studied. The boundary conditions are listed below in detail:

$$u^1\left(X^1, X^2, 0\right) = u^2\left(X^1, X^2, 0\right) = u^3\left(X^1, X^2, 0\right) = 0 \tag{88}$$

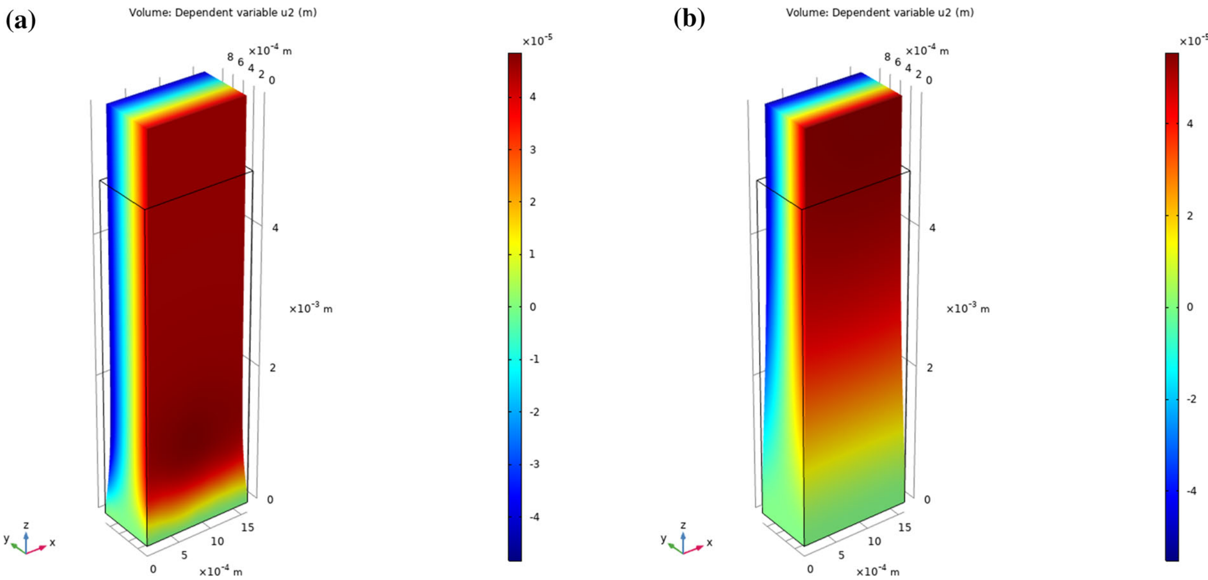

FIG. 6. Axial test: transversal displacement u_2 for material parameters of **a** Type 3 **b** Type 4

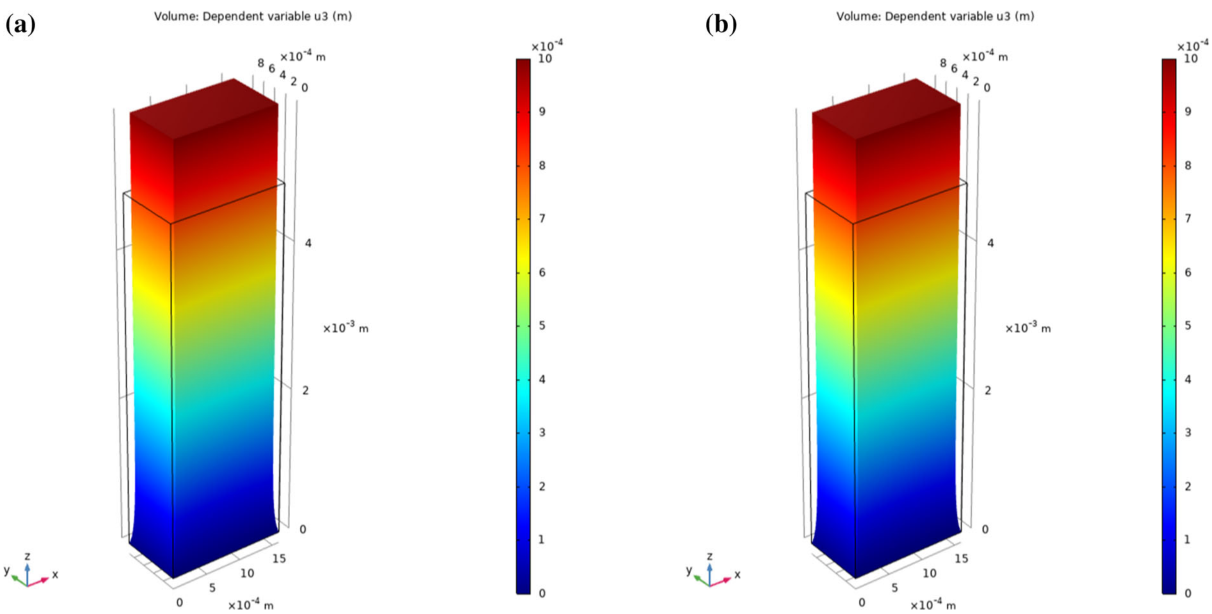

FIG. 7. Axial test: axial displacement u_3 for material parameters of **a** Type 1 **b** Type 2

$$r^1\left(X^1, X^2, 0\right) = r^2\left(X^1, X^2, 0\right) = r^3\left(X^1, X^2, 0\right) = 0 \tag{89}$$

$$u_1\left(X^1, X^2, l\right) = 1 \cdot 10^{-3}\,\mathrm{m} \tag{90}$$

The base b is fixed equal to 0.9 mm, the height h equal to 1.6 mm and the length l equal to 4.8 mm. It goes without saying that the description by means of the Euler angles is preferred (see Eq. (85)). In

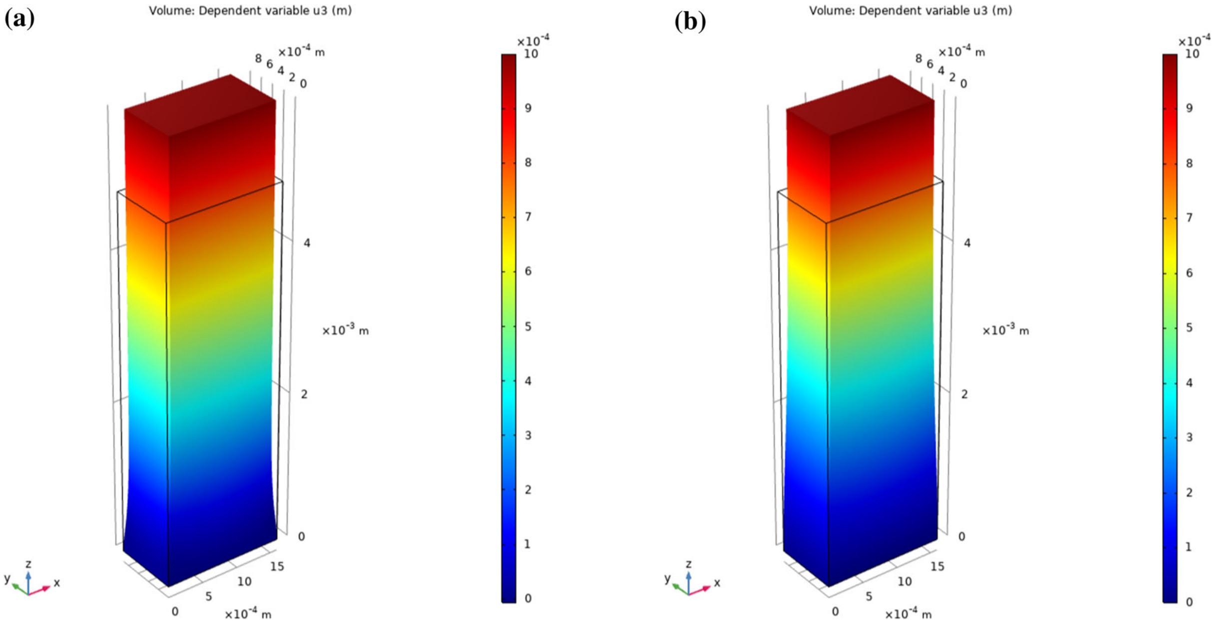

FIG. 8. Axial test: axial displacement u_3 for material parameters of **a** Type 3 **b** Type 4

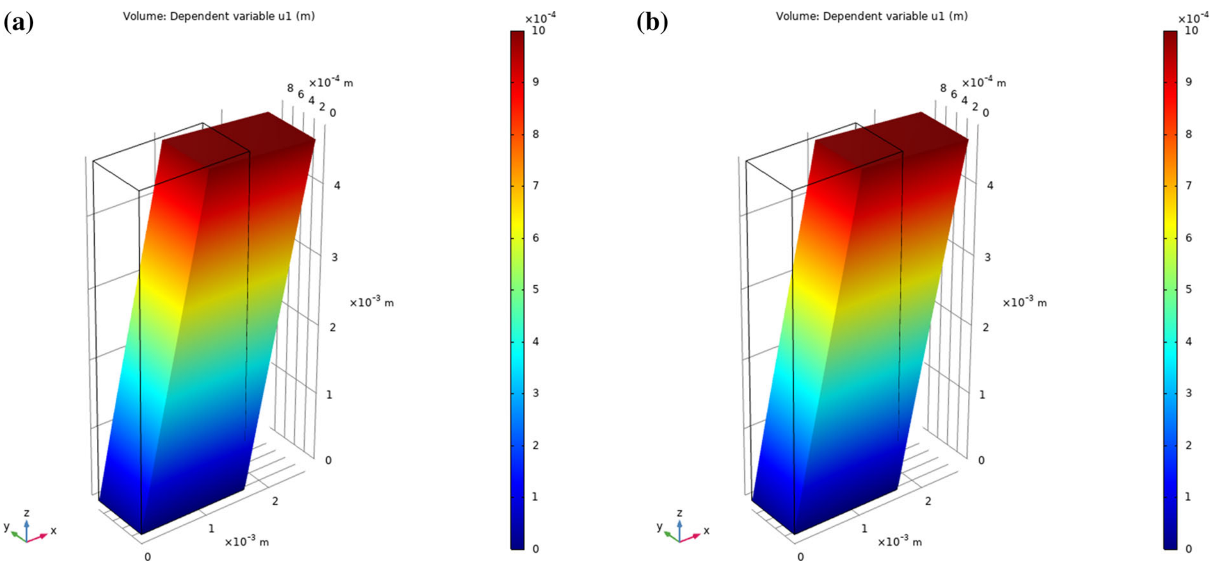

FIG. 9. Bending test: transversal displacement u_1 for material parameters of **a** Type 1 **b** Type 2

Figs. 9, 10, 11, 12 and 13, 14, the spatial distributions of the displacements u_1, u_2 and u_3 are analysed for the material parameters of Type 1, Type 2, Type 3 and Type 4 (see Table 1). The presence of the relative rotation tensor $\mathcal{R}$ acts on two main aspects. As the parameter $\xi_{\mathcal{R}}$ increases, the sign of the axial displacements u_3 change along the transversal sections with a consequent inversion of the stretched and compressed fibres. Where classical elasticity predicts traction, the presented model can

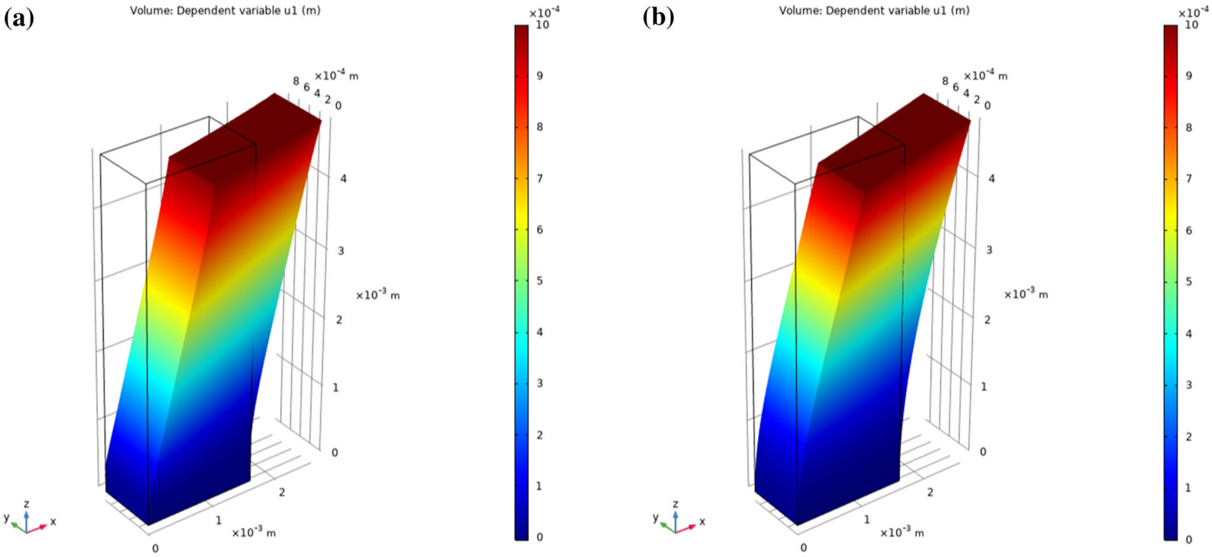

FIG. 10. Bending test: transversal displacement u_1 for material parameters of **a** Type 3 **b** Type 4

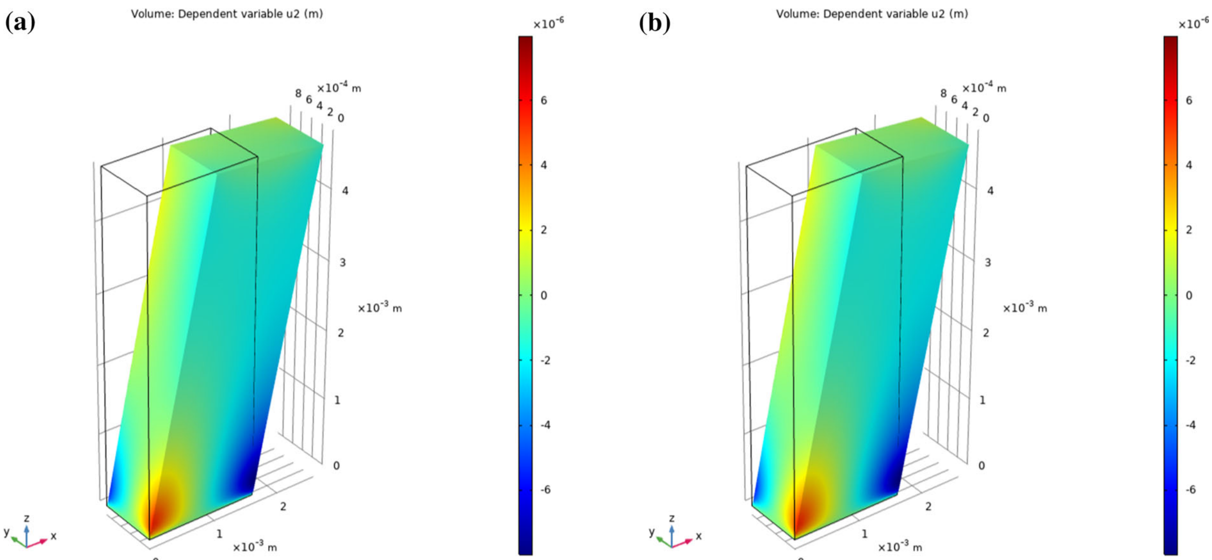

FIG. 11. Bending test: transversal displacement u_2 for material parameters of **a** Type 1 **b** Type 2

predict compression, and the extreme free section rotates counterclockwise instead of clockwise. Moreover, the portion of the beam affected by curvature decreases at the same time. The spatial distributions of u_1, u_2 and u_3, which are shown in Figure 9, 10, 11, 12, 13, 14, are closely related to the skewsymmetric part of the tensor $\mathcal{R}$.

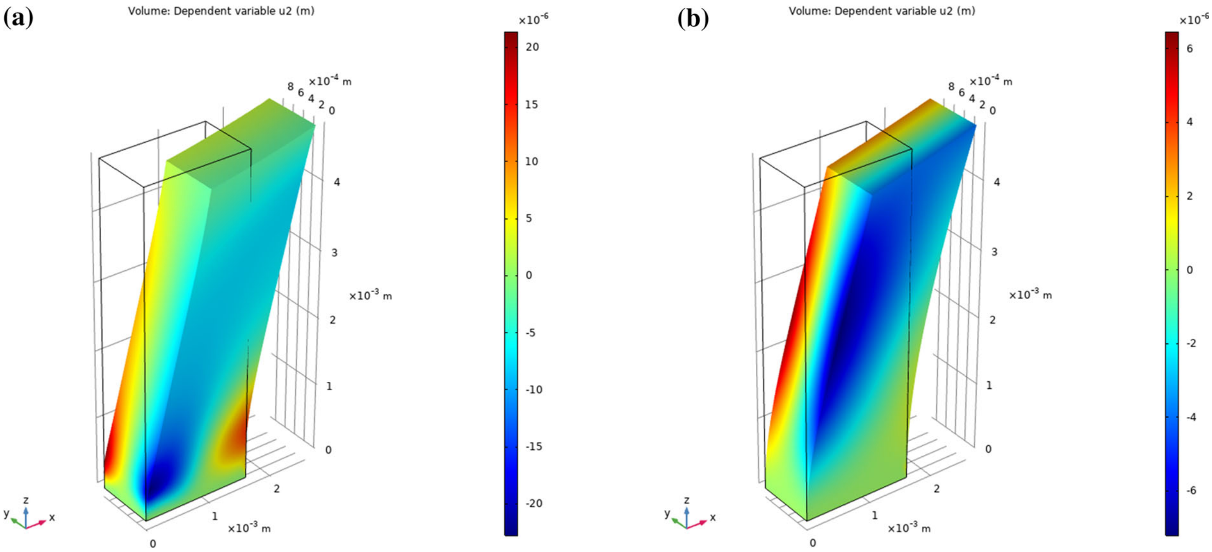

FIG. 12. Bending test: transversal displacement u_2 for material parameters of **a** Type 3 **b** Type 4

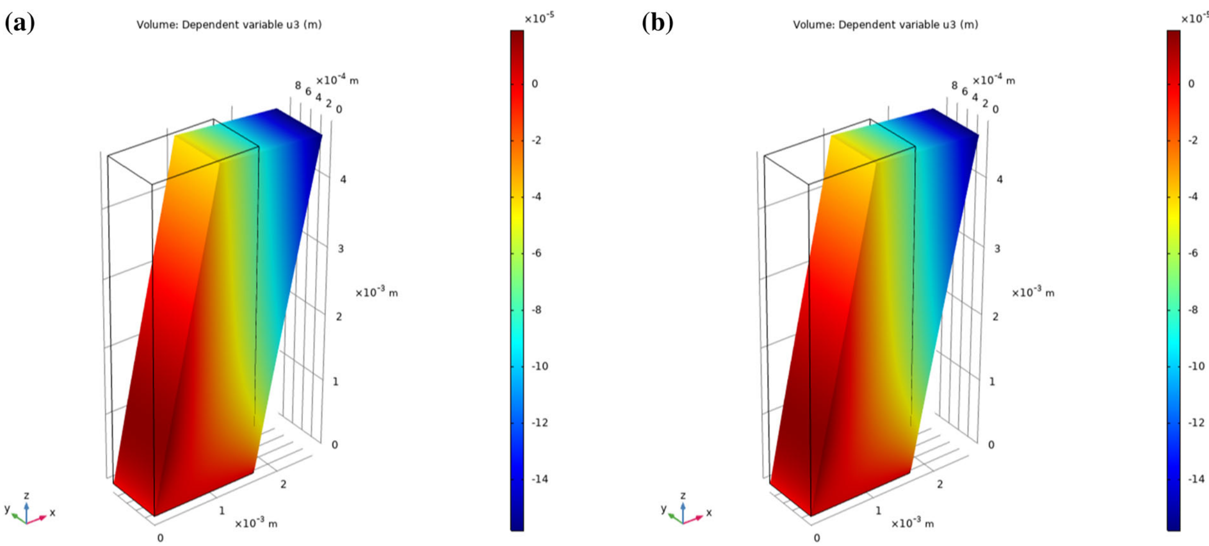

FIG. 13. Bending test: axial displacement u_3 for material parameters of **a** Type 1 **b** Type 2

4.4. Torsion test

In this section, a cylinder of radius $r = 4 \cdot 10^{-4}$ m and length $l = 10^{-3}$ m is studied. This kind of element can be thought as a pivot of a pantographic structure which is more subjected to torsional than to bending or axial deformations. Also in this case, a description of the microrotation tensor Q by means of angles (see Eq. (85)) is preferred. Below is a detailed list of the imposed boundary conditions:

$$u^1\left(0, X^2, X^3\right) = u^2\left(0, X^2, X^3\right) = u^3\left(0, X^2, X^3\right) = 0 \tag{91}$$

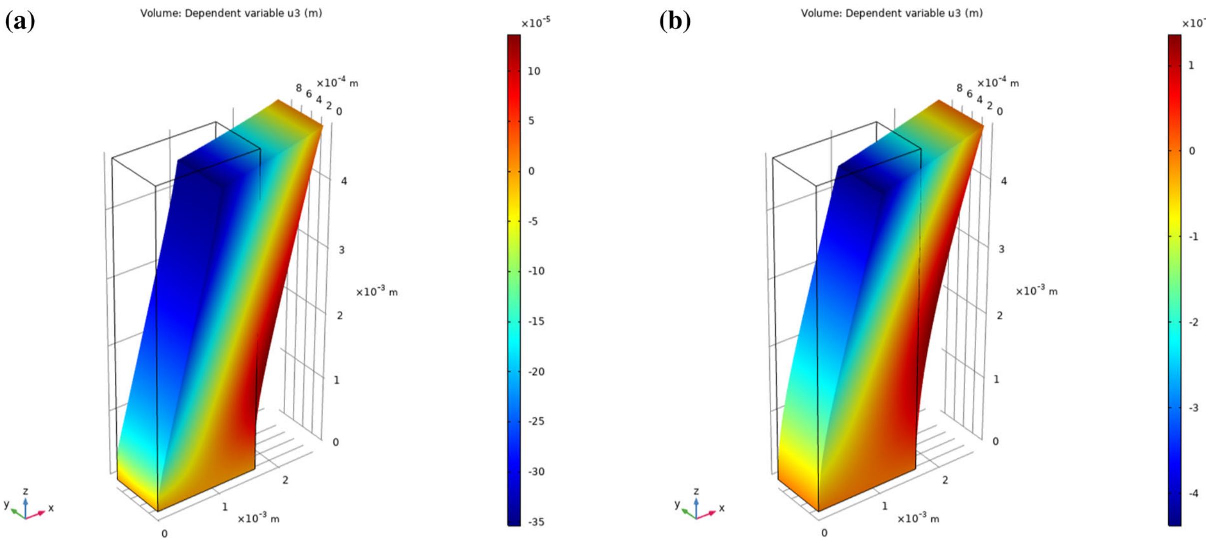

FIG. 14. Bending test: axial displacement u_3 for material parameters of **a** Type 3 **b** Type 4

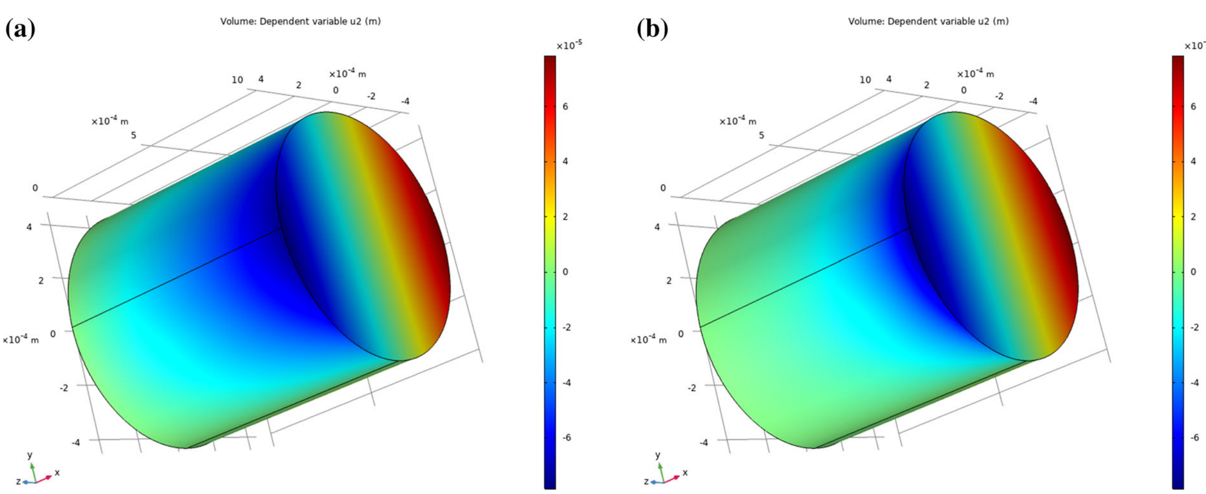

FIG. 15. Torsion test: transversal displacement u_2 for material parameters of (a) Type 1 (b) Type 2

$$r^1\left(0, X^2, X^3\right) = r^2\left(0, X^2, X^3\right) = r^3\left(0, X^2, X^3\right) = 0 \tag{92}$$

$$u_1\left(l, X^2, X^3\right) = 0 \tag{93}$$

$$u_2\left(l, X^2, X^3\right) = X^2 \cos\left(\theta - 1\right) - X^3 \sin\left(\theta\right) \tag{94}$$

$$u_3\left(l, X^2, X^3\right) = X^3 \cos\left(\theta - 1\right) + X^2 \sin\left(\theta\right) \tag{95}$$

A rotated reference system with respect to the previous numerical tests has been preferred by the author just for convenience. In Figs. 15, 16, the displacements u_2 and u_3 are evaluated for the material parameters of Type 1, Type 2 (see Table 1). The reported figures show that the presence of the deformation tensor $\mathcal{R}$ allows to reduce the part of the sample interested by values of u_2 and u_3 different from zero.

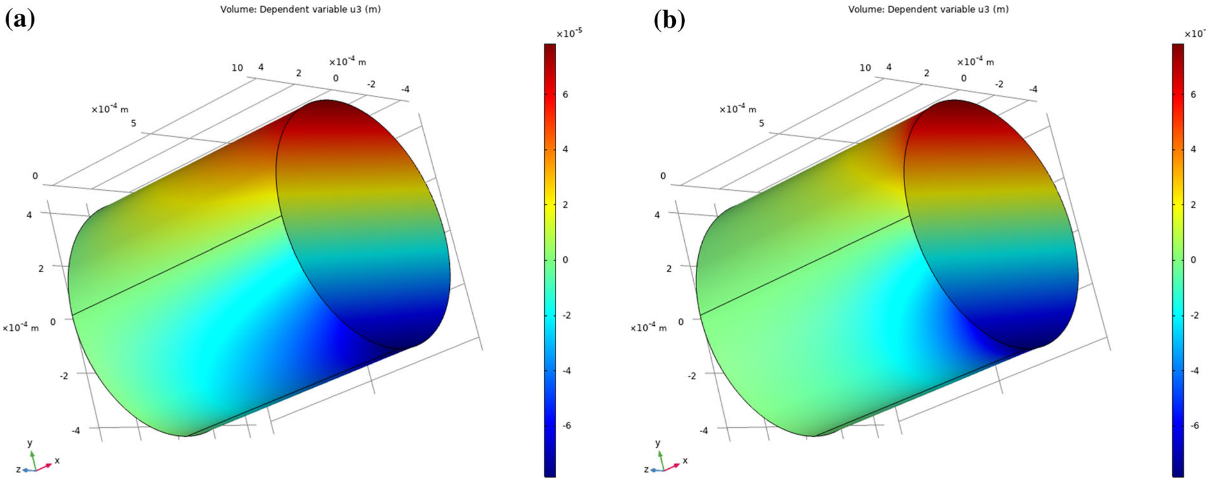

FIG. 16. Torsion test: axial displacement u_3 for material parameters of (a) Type 1 (b) Type 2

Conclusions

In this paper, a new deformation measure $\mathcal{R}$ for the nonlinear micropolar continuum is introduced. It takes into account the difference between micro- and macrorotations and it allows to clearly distinguish classic and non-classic energetic contributions. In addition to the new kinematic definition, the Euler–Lagrange equations are also derived by means of the least action principle and Levi–Civita absolute tensor calculus.

Some numerical applications are performed to analyse the mechanical implications of the proposed theoretical model. Typical substructures of pantographic sheets are studied by means of axial, bending and torsion numerical tests. The obtained results show some interesting effects as the constitutive parameter linked to the skewsymmetric part of the relative rotation tensor $\mathcal{R}$ increases: the transversal displacements of a rectangular beam subjected to a fixed axial displacement become progressively equal to zero; the position of the stretched and compressed fibres in a rectangular beam subjected to a transversal displacement becomes opposite to the ones provided by classical elasticity; the portion of a cylindrical beam characterized by transversal displacements equal to zero increases if a torsion is imposed; the portion of a rectangular beam characterized by curvature decreases if a transversal displacement is imposed. It is noteworthy, the relative rotation tensor $\mathcal{R}$ and the deformation energy density W^{def} proposed by the author (quadratic with respect to the Green–Saint–Venant tensor E, $\mathcal{R}$, the wryness tensor Γ and modelling an isotropic material) do not involve any kind of kinematic linearization; then, it holds whatever the amplitude of the imposed external loads, displacements and rotations. On the contrary, Eqs. (75–76) can be used only in the case of small displacements and rotations. The presented numerical applications seek to highlight the ability of the introduced model to derive large displacements and rotations solutions. Moreover, the proposed relative rotation tensor implies the possibility to assume the skewsymmetric part of the stretch tensor, denoted by $_A\bar{\mathcal{E}}$, as a measure of the micro/macro-relative rotation. The author believes that in the present paper, he has presented enough arguments to conclude that the new relative rotation tensor $\mathcal{R}$ is the most appropriate to describe the micro/macro-relative rotation effects in the field of nonlinear micropolar continua. Possible applications concern granular and compositebreak materials.

Declarations

Conflict of interest The author declares he has no conflict of interest.

Publisher's Note Springer Nature remains neutral with regard to jurisdictional claims in published maps and institutional affiliations.

References

[1] Cosserat, E., Cosserat, F.: Théorie des corps déformables. A. Hermann et Fils, Paris (1909)

[2] Eremeyev, V.A., Leonid, P., Altenbach, L.H.: Foundations of micropolar mechanics. Springer,, Berlin (2013). https://doi.org/10.1007/978-3-642-28353-6

[3] Altenbach, H., Eremeyev, V.A.: Generalized Continua from the Theory to Engineering Applications. Springer, Vienna (2013). https://doi.org/10.1007/978-3-7091-1371-4

[4] Altenbach, J., Altenbach, H., Eremeyev, V.A.: On generalized Cosserat-type theories of plates and shells: a short review and bibliography. Arch. Appl. Mech. **80**, 73–92 (2010). https://doi.org/10.1007/s00419-009-0365-3

[5] Forest, S.: Micromorphic media. In Altenbach, H., and Eremeyev, V.A. (eds.) Generalized continua from the theory to engineering applications (CISM International Centre for Mechanical Sciences, vol. 541), pp. 249–300. Springer, Vienna, Austria (2013)

[6] dell'Isola, F., Eremeyev, V.A.: Some introductory and historical remarks on mechanics of microstructured materials. In: dell'Isola, F., Eremeyev, V.A., Porubov, A. (eds.) Adv. Mech. Microstruct. Media Struct., pp. 1–20. Springer, Cham (2018)

[7] Eremeyev, V.A., Pietraszkiewicz, W.: Material symmetry group and constitutive equations of micropolar anisotropic elastic solids. Math. Mech. Solids (2015). https://doi.org/10.1177/1081286515582862

[8] Bersani, A., dell'Isola, F., Seppecher, P.: Lagrange multipliers in infinite dimensional spaces, examples of application (2019)

[9] dell'Isola, F., Di Cosmo, F.: Lagrange Multipliers in Infinite Dimensional Systems, Methods of. In: Altenbach, H., Ochsner, A. (eds.) Encyclopedia of Continuum Mech. Springer, Berlin (2018)

[10] dell'Isola, F., Maier, G., Perego, U., Andreaus, U., Forest, S., Esposito, R.: The complete works of Gabrio Piola: Volume I. Springer (2016). https://doi.org/10.1007/978-3-319-00263-7

[11] dell'Isola, F., Andreaus, U., Cazzani, A., Esposito, R., Placidi, L., Perego, U., Maier, G., Seppecher, P.: The complete works of Gabrio Piola: Volume II. Springer (2019). https://doi.org/10.1007/978-3-319-70692-4

[12] dell'Isola, F., Andreaus, U., Placidi, L.: At the origins and in the vanguard of peridynamics, non-local and higher-gradient continuum mechanics: An underestimated and still topical contribution of Gabrio Piola. Math. Mech. Solids **20**(8): 887-928 (2015). https://doi.org/10.1177/1081286513509811

[13] dell'Isola, F., Della Corte, A., Giorgio, I.: Higher-gradient continua: The legacy of Piola, Mindlin, Sedov and Toupin and some future research perspectives. Math. Mech. Solids **22**(4), 852–872 (2017). https://doi.org/10.1177/1081286515616034

[14] Spagnuolo M., Ciallella A., Scerrato D.: The loss and recovery of the works by piola and the italian tradition of mechanics. In: dell'Isola, F., Eugster, S.R., Spagnuolo, M., Barchiesi, E. (eds) Evaluation of Scientific Sources in Mechanics. Advanced Structured Materials, vol 152. Springer, Cham (2022). https://doi.org/10.1007/978-3-030-80550-0_4

[15] Auffray, N., dell'Isola, F., Eremeyev, V.A., Madeo, A., Rosi, G.: Analytical continuum mechanics à la Hamilton-Piola least action principle for second gradient continua and capillary fluids. Math. Mech. Solids **20**(4), 375–417 (2015). https://doi.org/10.1177/1081286513497616

[16] dell'Isola, F., Seppecher, P.: Edge contact forces and quasi-balanced power. Meccanica **32**, 33–52 (1997). https://doi.org/10.1023/A:1004214032721

[17] dell'Isola, F., Seppecher, P.: The relationship between edge contact forces, double forces and interstitial working allowed by the principle of virtual power. Comptes rendus de l'Académie des sciences. Série IIb, Mécanique, physique, astronomie, centre Mersenne, pp. 7 (1995)

[18] Seppecher, P.: Second-gradient theory: Application to Cahn-Hilliard fluids. In: Maugin G.A., Drouot R., Sidoroff F. (eds) Continuum Thermomechanics. Solid Mechanics and Its Applications, vol. 76. Springer, Dordrecht (2000). https://doi.org/10.1007/0-306-46946-4_29

[19] Andreaus, U., dell'Isola, F., Giorgio, I., Placidi, L., Lekszycki, L., Rizzi, N.L.: Numerical simulations of classical problems in two-dimensional (non) linear second gradient elasticity. Int. J. Eng. Sci. **108**, 34–50 (2016). https://doi.org/10.1016/j.ijengsci.2016.08.003

[20] Eugster, S.R., dell'Isola, F.: Exegesis of the introduction and sect. I from "Fundamentals of the Mechanics of Continua"** by E. Hellinger. Z. Angew. Math. Mech. **97**(4), 477–506 (2017). https://doi.org/10.1002/zamm.201600108

[21] Eugster, S.R., dell'Isola, F.: Exegesis of Sect. II and III.A from "Fundamentals of the Mechanics of Continua" by E. Hellinger. Z. Angew. Math. Mech. **98**(1), 31–68 (2018). https://doi.org/10.1002/zamm.201600293

[22] Eugster, S.R., dell'Isola, F.: Exegesis of Sect. III.B from "Fundamentals of the Mechanics of Continua" by E. Hellinger. Z. Angew. Math. Mech. **98**(1), 69–105 (2018). https://doi.org/10.1002/zamm.201700112

[23] Germain, P.: The method of virtual power in the mechanics of continuous media, I: Second-gradient theory. Math. Mech. Complex Syst. **8**(2), 153–190 (2020). https://doi.org/10.2140/memocs.2020.8.153

[24] Barchiesi E., Ciallella A., Scerrato D.: A partial report on the controversies about the principle of virtual work: from archytas of tarentum to lagrange, piola, mindlin and toupin. In: dell'Isola F., Eugster S.R., Spagnuolo M., Barchiesi E. (eds) Evaluation of Scientific Sources in Mechanics. Advanced Structured Materials, vol 152. Springer, Cham (2022). https://doi.org/10.1007/978-3-030-80550-0_5

[25] dell'Isola, F., Placidi, L.: Variational principles are a powerful tool also for formulating field theories. In: dell'Isola, F., Gavrilyuk, S. (eds) Variational Models and Methods in Solid and Fluid Mechanics. CISM Courses and Lectures, vol 535. Springer, Vienna (2011). https://doi.org/10.1007/978-3-7091-0983-0_1

[26] Ciallella, A.: Research perspective on multiphysics and multiscale materials: a paradigmatic case. Contin. Mech. Thermodyn. **32**, 527–539 (2020). https://doi.org/10.1007/s00161-020-00894-0

[27] dell'Isola, F., Seppecher, P., Alibert, J.J., et al.: Pantographic metamaterials: an example of mathematically driven design and of its technological challenges. Contin. Mech. Thermodyn. **31**, 851–884 (2019). https://doi.org/10.1007/s00161-018-0689-8

[28] dell'Isola, F., Steigmann, D., Della Corte, A.: Synthesis of fibrous complex structures: designing microstructure to deliver targeted macroscale response. Appl. Mech. Rev. **67**(6), 060804-1–21 (2016). https://doi.org/10.1115/1.4032206

[29] Turco, E., Giorgio, I., Misra, A., dell'Isola, F.: King post truss as a motif for internal structure of (meta) material with controlled elastic properties. R. Soc. Open Sci. (2017). https://doi.org/10.1177/1081286520978516

[30] Gołaszewski, M., Grygoruk, R., Giorgio, I., Laudato, M., Di Cosmo, F.: Metamaterials with relative displacements in their microstructure: technological challenges in 3Dprinting, experiments and numerical predictions. Contin. Mech. Thermodyn. **31**, 1015–1034 (2019). https://doi.org/10.1007/s00161-018-0692-0

[31] Barchiesi, E., Spagnuolo, M., Placidi, L.: Mechanical metamaterials: a state of the art. Math. Mech. Solids **24**(1), 212–234 (2018). https://doi.org/10.1177/1081286517735695

[32] Barchiesi, E., Placidi, L.: A review on models for the 3D statics and 2D dynamics of pantographic fabrics. In: Sumbatyan M. (eds) Wave dynamics and composite mechanics for microstructured materials and metamaterials. Advanced structured materials, vol. 59. Springer, Singapore (2017). https://doi.org/10.1007/978-981-10-3797-9_14

[33] Giorgio, I., Spagnuolo, M., Andreaus, U., Scerrato, D., Bersani, A.M.: In-depth gaze at the astonishing mechanical behavior of bone: A review for designing bio-inspired hierarchical metamaterials. Math. Mech. Solids **26**(6), 1074–1103 (2021)

[34] Alibert, J.-J., Seppecher, P., dell'Isola, F.: Truss modular beams with deformation energy depending on higher displacement gradients. Math. Mech. Solids **8**(1), 51–73 (2003). https://doi.org/10.1177/1081286503008001658

[35] dell'Isola, F., Giorgio, I., Pawlikowski, M. and Rizzi, N.L.: Large deformations of planar extensible beams and pantographic lattices: heuristic homogenization, experimental and numerical examples of equilibrium. Proc. R. Soc. A. 4722015079020150790 (2016). https://doi.org/10.1098/rspa.2015.0790

[36] dell'Isola, F., Seppecher, P., Spagnuolo, M., et al.: Advances in pantographic structures: design, manufacturing, models, experiments and image analyses. Contin. Mech. Thermodyn. **31**, 1231–1282 (2019). https://doi.org/10.1007/s00161-019-00806-x

[37] Eremeyev, V.A., dell'Isola, F., Boutin, C., Steigmann, D.: Linear pantographic sheets: existence and uniqueness of weak solutions. J. Elast. **132**, 175–196 (2018). https://doi.org/10.1007/s10659-017-9660-3

[38] Ciallella, A., Pasquali, D., Gołaszewski, M., D'Annibale, F., Giorgio, I.: A rate-independent internal friction to describe the hysteretic behavior of pantographic structures under cyclic loads. Mech. Res. Commun. **116**, 103761 (2021). https://doi.org/10.1016/j.mechrescom.2021.103761

[39] Giorgio, I.: Lattice shells composed of two families of curved Kirchhoff rods: an archetypal example, topology optimization of a cycloidal metamaterial. Continuum Mech. Thermodyn. **33**, 1063–1082 (2021). https://doi.org/10.1007/s00161-020-00955-4

[40] Greco, L.: An iso-parametric G^1-conforming finite element for the nonlinear analysis of Kirchhoff rod. Part I: the 2D case. Continuum Mech. Thermodyn. **32**, 1473–1496 (2020). https://doi.org/10.1007/s00161-020-00861-9

[41] Andreaus, U., Spagnuolo, M., Lekszycki, T., Eugster, S.R.: A Ritz approach for the static analysis of planar pantographic structures modeled with nonlinear Euler-Bernoulli beams. Contin. Mech. Thermodyn. **30**, 1103–1123 (2018). https://doi.org/10.1007/s00161-018-0665-3

[42] Turco, E., dell'Isola, F., Cazzani, A., Rizzi, N.L.: Hencky-type discrete model for pantographic structures: numerical comparison with second gradient continuum models. Z. Angew. Math. Phys. **67**(4), 1–28 (2016). https://doi.org/10.1007/s00033-016-0681-8

[43] Turco, E., dell'Isola, F., Cazzani, A., et al.: Hencky-type discrete model for pantographic structures: numerical comparison with second gradient continuum models. Z. Angew. Math. Phys. **67**, 85 (2016). https://doi.org/10.1007/s00033-016-0681-8

[44] Turco, E., Barchiesi, E., Giorgio, I., dell'Isola, F.: A Lagrangian Hencky-type non-linear model suitable for metamaterials design of shearable and extensible slender deformable bodies alternative to Timoshenko theory. Int. J. Nonlin. Mech. **123**, 103481 (2020). https://doi.org/10.1016/j.ijnonlinmec.2020.103481

[45] Turco, E., Misra, A., Pawlikowski, M., dell'Isola, F., François, H.: Enhanced Piola-Hencky discrete models for pantographic sheets with pivots without deformation energy: Numerics and experiments. Int. J. Solids Struct. **147**, 94–109 (2018). https://doi.org/10.1016/j.ijsolstr.2018.05.015

[46] Rahali, Y., Giorgio, I., Ganghoffer, J.F., dell'Isola, F.: Homogenization à la Piola produces second gradient continuum models for linear pantographic lattices. Int. J. Eng. Sci. **97**, 148–172 (2015). https://doi.org/10.1016/j.ijengsci.2015.10.003

[47] Giorgio, I.: Numerical identification procedure between a micro-Cauchy model and a macro-second gradient model for planar pantographic structures. Z. Angew. Math. Phys. **67**, 95 (2016). https://doi.org/10.1007/s00033-016-0692-5

[48] Misra, A., Poorsolhjouy, P.: Granular micromechanics based micromorphic model predicts frequency band gaps. Contin. Mech. Thermodyn. **28**(1–2), 215–234 (2016). https://doi.org/10.1007/s00161-015-0420-y

[49] Misra, A., Poorsolhjouy, P.: Identification of higher-order elastic constants for grain assemblies based upon granular micromechanics. Math. Mech. Complex Syst. **3**(3), 285–308 (2015). https://doi.org/10.2140/memocs.2015.3.285

[50] Misra, A., Poorsolhjouy, P.: Elastic behavior of 2D grain packing modeled as micromorphic media based on granular micromechanics. J. Eng. Mech. **143**(1), C4016005 (2016). https://doi.org/10.1061/(ASCE)EM.1943-7889.0001060

[51] Giorgio, I., De Angelo, M., Turco, E., et al.: A Biot-Cosserat two-dimensional elastic nonlinear model for a micromorphic medium. Contin. Mech. Thermodyn. **32**, 1357–1369 (2020). https://doi.org/10.1007/s00161-019-00848-1

[52] Giorgio, I., dell'Isola, F., Misra, A.: Chirality in 2D Cosserat media related to stretch-micro-rotation coupling with links to granular micromechanics. Int. J. Solids Struct. **202**, 28–38 (2020). https://doi.org/10.1016/j.ijsolstr.2020.06.005

[53] Turco, E., dell'Isola, F., Misra, A.: A nonlinear Lagrangian particle model for grains assemblies including grain relative rotations. Int. J. Numer. Anal. Meth. Geomech. **43**(5), 1051–1079 (2019). https://doi.org/10.1002/nag.2915

[54] Steigmann, D.: Theory of elastic solids reinforced with fibers resistant to extension, flexure and twist. Int. J. Non-Linear Mech. **47**, 734–742 (2012). https://doi.org/10.1016/j.ijnonlinmec.2012.04.007

[55] Shirani, M., Steigmann, D.: A cosserat model of elastic solids reinforced by a family of curved and twisted fibers. Symmetry **12**(7), 1133 (2020). https://doi.org/10.3390/sym12071133

[56] Trovalusci, P., Ostoja-Starzewski, M., De Bellis, M.L., Murrali, A.: Scale-dependent homogenization of random composites as micropolar continua. Eur. J. Mech. A/Solid **49**, 396–407 (2015). https://doi.org/10.1016/j.euromechsol.2014.08.010

[57] Falsone, G., Impollonia, N.: A new approach for the stochastic analysis of finite element modelled structures with uncertain parameters. Comput. Methods Appl. Mech. Eng. **191**, 5067–5085 (2002). https://doi.org/10.1016/S0045-7825(02)00437-1

[58] Falsone, G., Impollonia, N.: About the accuracy of a novel response surface method for the analysis of finite element modeled uncertain structures. Probab. Eng. Mech. **19**, 53–63 (2004). https://doi.org/10.1016/j.probengmech.2003.11.005

[59] Falsone, G., Ferro, G.: A dynamical stochastic finite element method based on the moment equation approach for the analysis of linear and nonlinear uncertain structures. Struct. Eng. Mech. **23**, 599–613 (2006). https://doi.org/10.12989/sem.2006.23.6.599

[60] Soize, C.: Non-Gaussian positive-definite matrix-valued random fields for elliptic stochastic partial differential operators. Comput. Methods Appl. Mech. Eng. **195**, 26–64 (2006). https://doi.org/10.1016/j.cma.2004.12.014

[61] La Valle, G., Laudani, R., Falsone, G.: Response probability density function for non-bijective transformations. Commun. Nonlinear Sci. Numer. Simulat. (2022). https://doi.org/10.1016/j.cnsns.2021.106190

[62] Falsone, G., Laudani, R.: Multi-time probability density functions of the dynamic non-Gaussian response of structures. Struct. Eng. Mech. **76**, 631–641 (2020)

[63] Falsone, G., Settineri, D.: On the application of the probability transformation method for the analysis of discretized structures with uncertain properties. Probab. Eng. Mech. **35**, 44–51 (2014). https://doi.org/10.1016/j.probengmech.2013.10.001

[64] Falsone, G., Laudani, R.: A probability transformation method (PTM) for the dynamic stochastic response of structures with non-Gaussian excitations. Eng. Comput. **35**, 1978–1997 (2018). https://doi.org/10.1108/EC-12-2017-0518

[65] Laudani, R., Falsone, G.: Use of the probability transformation method in some random mechanic problems. ASCE-ASME J. Risk Uncertain. Eng. Syst. (2021). https://doi.org/10.1061/AJRUA6.0001111

[66] Falsone, G., Laudani, R.: Exact response probability density functions of some uncertain structural systems. Arch. Mech. **71**, 315–336 (2019)

[67] Falsone, G., Laudani, R.: Matching the principal deformation mode method with the probability transformation method for the analysis of uncertain systems. Int. J. Num. Methods Eng. **118**, 395–410 (2019). https://doi.org/10.1002/nme.6018

[68] Pietraszkiewicz, W., Eremeyev, V.A.: On natural strain measures of the non-linear micropolar continuum. Int. J. Solids Struct. **46**(3–4), 774–787 (2009). https://doi.org/10.1016/j.ijsolstr.2008.09.027

[69] Pietraszkiewicz, W., Eremeyev, V.A.: On vectorially parameterized natural strain measures of the non-linear Cosserat continuum. Int. J. Solids Struct. **46**(11–12), 2477–2480 (2009). https://doi.org/10.1016/j.ijsolstr.2009.01.030

[70] Zubov, L.M., Rudev, A.N.: Phys.-Dokl. (Russia) **41**, 544–547 (1996) (Trans. from Doklady Akademii Nauk 351, 188–191(1996))

[71] Bouby, C., Fortuné, D., Pietraszkiewicz, W., Vallée, C.: Direct determination of the rotation in the polar decomposition of the deformation gradient by maximizing a Rayleigh quotient. Z. Angew. Math. Mech. **85**, 155–162 (2005). https://doi.org/10.1002/zamm.200310167

[72] Bichara, A., dell'Isola, F.: Elementi di algebra tensoriale con applicazioni alla meccanica dei solidi. Progetto Leonardo, Bologna (2005)

[73] Misra, A., Placidi, L., dell'Isola, F., Barchiesi, E.: Identification of a geometrically nonlinear micromorphic continuum via granular micromechanics. Z. Angew. Math. Phys. **72**, 1–21 (2021). https://doi.org/10.1007/s00033-021-01587-7

[74] Svendsen, B., Bertram, A.: On frame-indifference and form-invariance in constitutive theory. Acta Mech. **132**, 195–207 (1999). https://doi.org/10.1007/BF01186967

[75] Neff, P., Jeong, J.: A new paradigm: the linear isotropic Cosserat model with conformally invariant curvature energy. Z. Angew. Math. Mech. **89**, 107–122 (2009). https://doi.org/10.1002/zamm.200800156

Gabriele La Valle
University of Messina
Messina Sicilia
Italy
e-mail: gabrielelavalle@gmail.com

(Received: October 1, 2021; revised: February 18, 2022; accepted: February 18, 2022)